The nano-structural characterization of Ω and S phases in Al-5.1Cu-1.0Mg-(0.4Ag) AA2024 aluminum alloys

Cheng-Ling Tai[a], Mien-Chung Chen[b], Tsai-Fu Chung[c], Yo-Lun Yang[d], Sheng-Long Lee[b], Tzu-Ching Tsao[a], Zhusheng Shi[e], Jianguo Lin[e], Te-Cheng Su[a], Hsueh-Ren Chen[a], Jer-Ren Yang[a,*]

[a] Department of Materials Science and Engineering, National Taiwan University, Taipei, Taiwan.
[b] Institute of Material Science and Engineering, National Central University, Taoyuan, Taiwan
[c] Department of Materials Science and Engineering, National Yang Ming Chiao Tung University, Hsinchu, Taiwan.
[d] Department of Mechanical Engineering, National Taipei University of Technology, Taipei, Taiwan
[e] Department of Mechanical Engineering, Imperial College London, London SW7 2AZ, UK

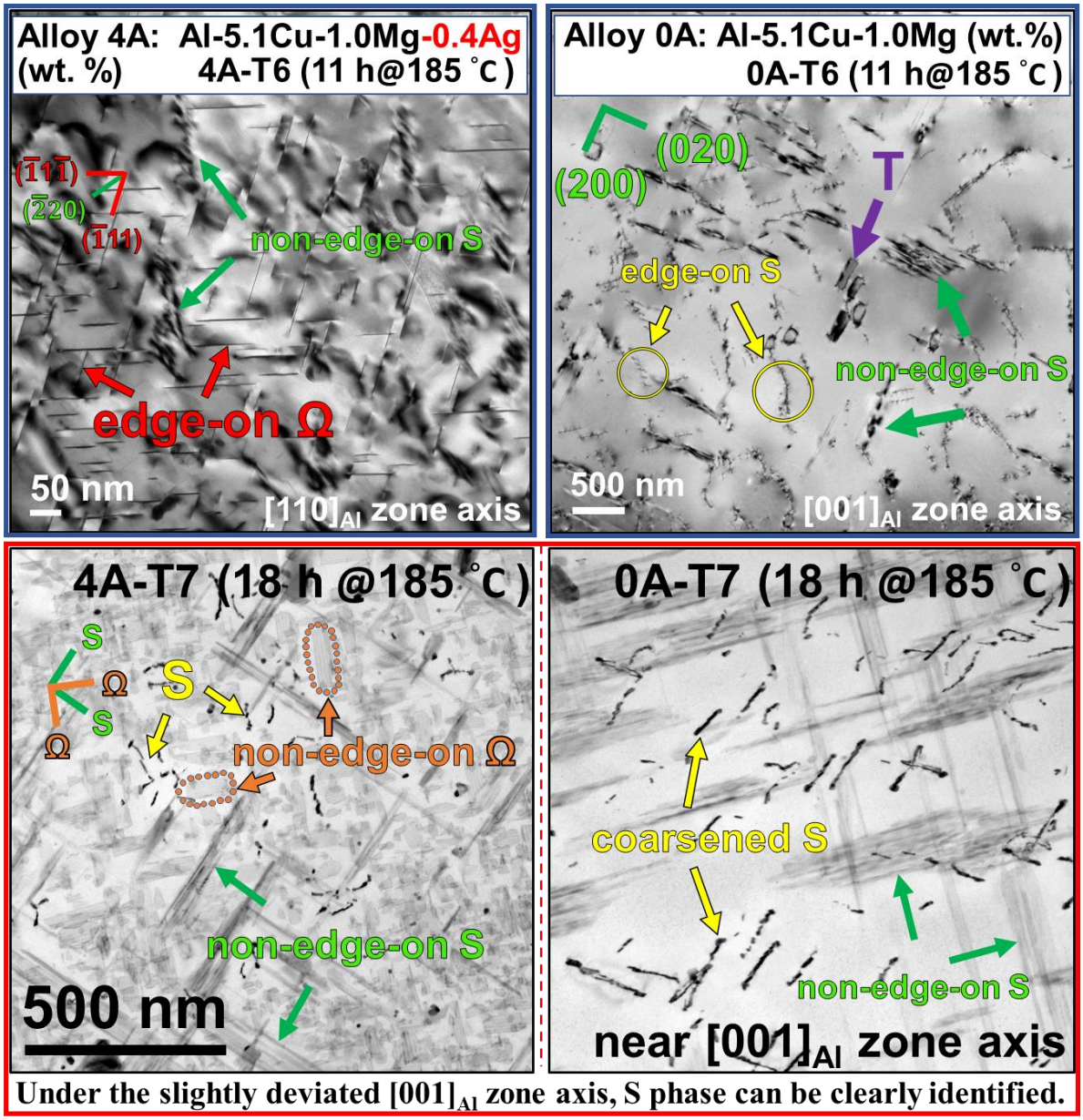
*Corresponding author: Jer-Ren Yang

Tel: +886–2–33661314

Fax: +886–2–23634562

E-mail of Corresponding author: jryang@ntu.edu.tw (J-R Y)

Graphical Abstract



Under the slightly deviated $[001]_{Al}$ zone axis, S phase can be clearly identified.

Highlights:

1. The microstructural evolutions and mechanical properties of both Ag-free (denoted as Alloy 0A) and 0.4 wt.% Ag-containing (denoted as Alloy 4A) AA2024 alloys treated at 185 °C for 5, 11, 18, and 100 h have been investigated.
2. In the peak ageing condition, the UTS of Alloy 4A is 16 % higher than that of Alloy 0A; this is associated with the former possessing the highly-dense and uniformly-distributed Ω phase.
3. TEM results provide evidence to suggest that the Ω phase was triggered by Ag addition, thereby the coarsening of the S phase being suppressed during a longer holding time from peak ageing to over-ageing treatment.
4. HR-STEM studies show that after ageing treatment at 185 °C for 100 h, the thermally stable Ω phase maintains a thickness of ~3 nm in Alloy 4A, and the corresponding UTS of Alloy 4A is ~38% higher than that of Alloy 0A.
5. Morphologies of non-edge-on Ω phase and S phase have also been investigated.

Abstract

The effects of a minor addition (0.4 wt.%) of Ag to Al-5.1Cu-1.0Mg aluminum alloy on the microstructural evolution and mechanical properties have been investigated. The under-ageing, peak ageing, over-ageing, and prolonged ageing at 185 °C were studied for the alloys with and without Ag additions to further correlate the microstructure with mechanical properties. The faster increment of hardness during the early stage (1-5 h) and much higher ultimate tensile strength (530 Mpa) at peak ageing condition in Ag-containing specimen were attributed to the formation of the Ω phase triggered by the Ag addition. In over-aged specimens, the S phase in the Ag-free specimen coarsened significantly, whereas the S phase in the Ag-containing specimen remained nearly the same size as that in its peak-ageing treated specimen. The formation of the Ω phase in the Ag-containing specimen presumably consumed the same solute atoms as the S phase, i.e., Cu and Mg, leading to the depleted zones of Cu-Mg in the aluminum matrix and thus suppressing the coarsening of the S phase during the ageing time from 11 h (peak ageing) to 18 h (over ageing). After ageing for 100 h (prolonged ageing), the S phase coalesced in both alloys. However, the Ω phase in the Ag-containing specimen still maintained a thickness of ~3 nm with a high level of volume percent (2.74 vol. %), which contributed significantly to the UTS (449 MPa).

Keywords: AA2024 aluminum alloys; Minor Ag addition; Thermally stable Ω phase; Suppression of S phase; High resolution transmission electron microscopy.

1. Introduction

2xxx aluminum alloys have been widely used in the automotive, aerospace, and defense industries due to their high specific strength and good fracture toughness [1-3]. In these aluminum alloys, highly-dense and uniformly-distributed nano-precipitates, which contribute to the high strength, are produced by suitable ageing treatments [4]. The conventional 2xxx (Al-Cu-Mg) aluminum alloys are strengthened by precipitates of the θ' phase (Al_2Cu) and S phase (Al_2CuMg); the former usually possesses a plate-like morphology, and the latter, a rod or lath-shaped morphology [5]. It has been suggested [5-10] that with different Cu/Mg ratios (wt.% is used in this study unless otherwise specified) in Al-Cu-Mg alloys, either the θ' phase (high Cu/Mg ratio > ~13) or the S phase (low Cu/Mg ratio < ~6) would dominate (competing with each other when 6 < Cu/Mg ratio < 13).

For advanced applications requiring higher strength and elevated temperature resistance, AA2040 Al-Cu-Mg-Ag aluminum alloys have been developed [6, 11-15]. In addition to the θ' and S phases, the development of the disc-shaped Ω phase (Al_2Cu), the interface of which segregates Mg and Ag, has attracted much attention due to its significant contribution to the mechanical strength of Al-Cu-Mg alloys [11-22]. It is significant that the addition of Ag plays an important role on the microstructural development of Al-Cu-Mg alloys. For example, a previous work has indicated [13] that an addition of 0.6 %Ag to Al-2.3Cu-1.6Mg-1.1Fe-1.0Ni-0.18Si-0.07Ti (wt.%)alloy increases the yield strength by 55% and the ultimate tensile strength

by 20%; this increment is attributed to the formation of highly dense nano-precipitates of the Ω phase. The Ω phase has been presumed to form on the $\{111\}_{Al}$ habit planes after the addition of trace amounts of Ag to Al-Cu-Mg alloys [11, 16-18]. In addition, it has been indicated that the average thickness of the Ω phase in the Al-4.0Cu-0.3Mg-0.4Ag alloy may be linearly related to the square root of ageing time ($h^{1/2}$, where h is ageing time in hours) [19]. Whenever ageing temperatures are below 200 °C, the slopes of ageing time (on x-axis) versus the thickness of the Ω phase (on y-axis) curves are very small. Even after ageing at 200 °C for 1000 h, the average thickness is less than 6 nm, indicating excellent thermal stability at elevated temperatures. Nevertheless, in a previous work [14] on Al-5.74Cu-0.44Mg-1.00Ag-0.27Mn-0.16Zr-0.05Ti (wt.%) alloy, although the thickness of the Ω phase remained nearly constant after treatment at 165 °C for 2 h followed by 200 °C for 1000 h, the length of the Ω phase increased (~45 %) with decreasing number density (~63 %), resulting in a decrease in UTS (~31.5%). A previous work [20] investigating the Al-2.5Cu-0.5Mg-0.5Ag (wt.%) alloy claimed that the Ω phase transformed into the equilibrium phase, the θ phase, after being aged at 200 °C for around 100 days. On the other hand, another work [19] on the Al-4.0Cu-0.3Mg-0.4Ag (wt.%) alloy reported that the Ω phase → θ phase transformation occurred when the samples were aged at 300 °C for 10 h. Therefore, adopting a proper ageing treatment (temperature and holding time) to control the size and quantity of the Ω phase is an essential work. During ageing at 200 °C, the Ω phase might not coarsen, but the strength will decrease because the quantity of

the Ω phase may be reduced, as seen in a previous work [21] on Al-5.6Cu-0.72Mg-0.5Ag-0.32Mn-0.17Sc-0.12Zr-0.1Ge (wt.%) alloy aged at 200 °C for over 2 h. In another previous work on Al-4.Cu-0.80Mg-0.14Ag-0.26Mn-0.16Zr (wt.%) alloy [22], the peak ageing condition required a long period (38 h) to achieve when the alloy was aged at 165 °C. In an investigation of Al-5.3Cu-0.8Mg-0.6Ag-0.2Zr (wt.%) alloy [23], it was reported that ageing at 185 °C for 12 h could achieve the peak ageing condition (with a hardness of 161 HV). The ageing temperature of 185 °C was also adopted in the present work so that the appropriate thickness of the Ω phase could be maintained during the ageing treatment, while the holding time for reaching the peak ageing was also expected to be on a suitable time scale.

The general evolution process involving the Ω phase in Al-Cu-Mg-Ag aluminum alloys is speculated as follows: SSSS → Ag-Mg cluster → $\{111\}_{Al}$ GP zone → Ω' phase → Ω phase → θ phase [24-28], where SSSS is a supersaturated solid solution. Heating to high temperatures causes the alloy additions to be solid-solutioned back into the aluminum matrix, and subsequent rapid water-cooling to room temperature leads to the formation of a supersaturated solid solution with considerable amounts of point defects (vacancies) to facilitate subsequent precipitation. It has been reported [9, 26, 29-31] that the Ω phase has an orthorhombic structure with a space group of Fmmm (a = 0.859 nm, b = 0.848 nm and c = 0.496 nm) and forms on the $\{111\}_{Al}$ habit planes. These Ω crystals have been presumed to possess 12 equivalent variants [9], and their orientation relationships with the aluminum matrix can be

described by $(001)_{\Omega}$ // $\{1\bar{1}1\}_{Al}$ and $[010]_{\Omega}$ // $<110>_{Al}$ [9, 29], as shown in Table 1. On the other hand, it is reported [32, 33] that, with the segregation of Mg and Ag at the interface between Ω and aluminum matrix, the Ω phase is presumed to be a meta-stable phase, which possesses elastic distortion at the interface. The Ω phase eventually transforms to the equilibrium θ phase, which has a tetragonal structure with a space group of I4/mcm, where a = 0.607 nm and c = 0.487 nm [34]. The θ' phase is the other meta-stable phase related to the θ phase; both possess the same $(001)_{Al}$ habit plane and crystal structure. The θ' phase has been reported to be a tetragonal structure with a space group of I4/mcm, where a = 0.404 nm and c = 0.580 nm [6], but to possess a different morphology from the θ phase (θ' phase: plate-like, θ phase: rod-like) [35, 36]. The phase transition from the θ' phase to the θ phase in Ag-free Al-Cu-Mg alloys is unclear, and that from the Ω phase with $\{111\}_{Al}$ habit planes to θ phase with $\{001\}_{Al}$ habit planes in Ag-containing Al-Cu-Mg alloys also remains a question. In one investigation of the Ω phase, it has been claimed [9] that no Ω phase is found in Al-4.0Cu-0.3Ag (wt.%) alloy without Mg addition; however, a very small amount of the Ω phase can still be found in Al-1.7Cu-0.3Mg (wt.%) alloy when it is treated at 180 °C for 2.5 h [26]. This difference apparently implies that Mg is a necessary element to form the Ω phase. Moreover, it has also been suggested that, when Ag is added to Al-Cu-Mg alloys (Al-3.0Cu-0.5Mg-0.5Ag, wt.%), the Ag acts as a catalyst to facilitate the formation of the Ω phase [30]. It has been claimed that Ag diffuses into the Mg-vacancies, decreasing the energy barrier of the Ω phase nucleation [9] and

also reducing the misfit energy between the Ω phase and the aluminum matrix [27]. Those effects presumably accelerate the generation of the Ω phase and make it abundantly and uniformly distributed in the aluminum matrix, thereby enhancing the strength of Al-Cu-Mg-Ag aluminum alloys [5, 9, 37, 38].

Table 1. Orientation relationships between Ω phase and aluminum matrix [9, 29].

12 equivalent variants of Ω phase	
$(001)_{\Omega}$ // $(111)_{Al}$	$[010]_{\Omega}$ // $[1\bar{1}0]_{Al}$
	$[010]_{\Omega}$ // $[10\bar{1}]_{Al}$
	$[010]_{\Omega}$ // $[0\bar{1}1]_{Al}$
$(001)_{\Omega}$ // $(\bar{1}11)_{Al}$	$[010]_{\Omega}$ // $[110]_{Al}$
	$[010]_{\Omega}$ // $[101]_{Al}$
	$[010]_{\Omega}$ // $[01\bar{1}]_{Al}$
$(001)_{\Omega}$ // $(1\bar{1}1)_{Al}$	$[010]_{\Omega}$ // $[110]_{Al}$
	$[010]_{\Omega}$ // $[10\bar{1}]_{Al}$
	$[010]_{\Omega}$ // $[011]_{Al}$
$(001)_{\Omega}$ // $(11\bar{1})_{Al}$	$[010]_{\Omega}$ // $[1\bar{1}0]_{Al}$
	$[010]_{\Omega}$ // $[101]_{Al}$
	$[010]_{\Omega}$ // $[011]_{Al}$

It is a view point [39] that, compared with Cu, Ag has a larger electronegativity difference with Mg and can more effectively trap Mg atoms to form a more stable cluster. Therefore, Al-Cu-Mg-Ag aluminum alloys are presumed more likely to form Ag-Mg clusters as nucleation sites for the subsequent phase precipitation of Ω phase. In an investigation employing atom probe tomography [24], it has been revealed that Cu atoms gradually diffuse into the Ag-Mg cluster at the beginning of artificial ageing to form GP zones on the $\{111\}_{Al}$ plane, with the

level of Cu increasing up to 20–25 at.% at this stage. On the other hand, the recent work on Al-6.4Cu-0.45Mg-0.4Ag-0.3Mn-0.15Zr (wt.%) alloy [28] proposed an evidence via HR-STEM images with atomic resolution energy dispersive X-ray spectroscopy (EDS) mapping to assert the existence of Ω' phase, the precursor of the Ω phase. This work claimed that the Ω' phase transited to the Ω phase by in-situ transformation mechanism. The possible formation mechanism of the Ω phase can be suggested as follows. During ageing at a proper temperature, the Cu atoms continue to diffuse into the precursor [24, 40]. Meanwhile, Ag and Mg diffuse to the boundary [24, 41], reducing the misfit strain energy and increasing the coherency with the $\{111\}_{Al}$ plane of aluminum matrix [15], and they eventually transform into the Ω phase. In a previous investigation of the Ω phase in Al-4.0Cu-0.3Mg-1.0Ag-0.1Si (wt.%) [32] and Al-4.0Cu-0.3Mg-0.4Ag (wt.%) alloys [31], Ag and Mg layers at the boundary of the Ω phase were confirmed by HADDF-STEM and EELS mapping. It is appropriate to conclude that the Ag and Mg atoms diffusing to the boundary of the Ω phase suppress its coarsening [33], facilitating an Ω phase with a high aspect ratio on the $\{111\}_{Al}$ habit plane. Previous works [42, 43] have asserted that the significant contribution of the Ω phase to the strengths at the room temperature and elevated temperature is basically due to its semi-coherent boundary with the $\{111\}_{Al}$ plane of the aluminum matrix, as the dislocations cut through the Ω phase during deformation. A previous work [44] more clearly pointed out that the Ω phase lying on the $\{111\}_{Al}$ plane provides only 75 % of the effective number density for blocking dislocation movement. This

viewpoint can be illustrated as follows. When the dislocations glide on one of four $\{111\}_{Al}$ slip planes in a face-centered cubic (FCC) aluminum structure, which is parallel to the corresponding $\{111\}_{Al}$ habit plane of the Ω phase, they will not effectively intersect with the Ω phase. When the dislocations glide on the other three $\{111\}_{Al}$ slip planes, however, intersections between the dislocations and the thin-platelet Ω phase do occur. In spite of the unclear strengthening mechanism of Ω phase, this phase is presumed to have a better strengthening ability than that of the θ' phase in high Cu / Mg ratio Al-Cu-Mg-Ag aluminum alloys [21].

Since Mg has a large influence on the formation of the Ω phase, variation of the Mg content appears to be one of the key factors in the alloy design of Al-Cu-Mg(-Ag) aluminum alloys. It has been claimed [45] that a high ratio (12.5) and a low ratio (4.1) of Cu/Mg in Al-5.0Cu-0.4Mg-1.1Ag-0.3Mn-0.16Zr (wt.%) alloy and Al-4.9Cu-1.2Mg-1.0Ag-0.3Mn-0.15Zr (wt.%), respectively, would yield a lower number density of Ag-Mg clusters in the early stage of artificial ageing at 165 °C, as observed by atom probe tomography, and thus reduce the strength of the materials. The highest strengths have been achieved at a suitable Cu/Mg ratio of 6.1 in Al-4.9Cu-0.8Mg-1.1Ag-0.3Mn-0.15Zr (wt.%) alloy [45] and a Cu/Mg ratio of 5.1 in Al-5.1Cu-1.0Mg-0.6Ag (wt.%) alloy [46]; nevertheless, the exact Cu/Mg ratio in Al-Cu-Mg-Ag alloys for achieving the highest strength should be further investigated. A previous work [5] has suggested that in Al-Cu-Mg aluminum alloys, rod or lath S-phase acts as the main strengthening precipitate when the Cu/Mg ratio is lower than 5. The high Cu/Mg ratio (~13) alloys, e.g.,

AA2519, with θ' phase as the strengthening phase, possess a good combination of stress corrosion resistance and weldability; in contrast, the low Cu/Mg ratio (~6) alloys, e.g., AA2024, with S phase, have even higher strength and toughness [47-50]. Although the addition of Ag promotes the formation of the Ω phase, the S phase may still be an important precipitate for strengthening Al-Cu-Mg-Ag aluminum alloys with low Cu/Mg ratio. Considering that the effect of the S phase coupled with the Ω phase has seldom been investigated in previous works, the present study attempted to explore this aspect in more detail.

In 1952, Bagaryastsky [51] first proposed the sequence of S phase evolution in Al-3Cu-1.5Mg aluminum alloys by X-ray scattering as follows: SSSS → GPB zones → GPB2/ S" → S' → S. In that evolutionary sequence, the Guinier-Preston-Bagaryatsky (GPB) zone was assumed to be a short-range order structure composed of Cu and Mg. The existence of GPB2 or S", a precursor of S' phase, remains under debate because other works [52, 53] have shown no evidence of it. The meta-stable S' phase and the equilibrium S phase are orthorhombic structures and have the same elemental composition, with only slight differences in the lattice constants [51]. In addition, the S phase not only evolves from the Cu-Mg cluster in the aluminum matrix but also heterogeneously nucleates on the dislocations and at the interfaces between the aluminum matrix and the T phase ($Al_{20}Cu_2Mn_3$), the latter being a dispersoid triggered by Mn addition [54, 55].

In recent works, the S phase evolution process in Al-Cu-Mg aluminum alloys has been adjusted as follows: SSSS → Cu-Mg cluster → GPB zones → S phase [26, 53, 56, 57]. The related transitions have been proposed and can be briefly described below. In the natural ageing stage, Cu-Mg clusters form due to the diffusion of atoms and vacancies. With artificial ageing heat treatment, Cu-Mg clusters gradually transform into GPB zone and then S phase. The S phase has an orthorhombic structure with a space group of Cmcm (a = 0.400 nm, b = 0.923 nm, c = 0.714 nm) growing on the $\{012\}_{Al}$ habit planes with 12 equivalent variants [58, 59], and its nominal chemical composition is presumed to be Al_2CuMg [26, 53, 56, 57]. The S phase has an orientation relationship with the Al matrix as follows: $(0\ 0\ 1)_S$ // $\{0\ 1\ 2\}_{Al}$ and $[1\ 0\ 0]_S$ // $<1\ 0\ 0>_{Al}$ [51, 60]. Previous works [61, 62] claimed the existence of two types of S phase in Al-2.5Cu-1.5Mg (wt.%) aluminum alloys, i.e., SI and SII. The former, SI, previously considered a meta-stable S' phase, is lath-shaped with a sharp boundary; in contrast, SII, the equilibrium S phase, is rod-shaped with a stepped boundary. Some other works suggested [63, 64] that the variation of Cu content brought about these two different types of S phase. They supposed that the SII phase contained a higher level of Cu than that of the SI phase, leading to differences in the lattice constants, but both were classified as the S phase rather than the S' phase.

In previous works on Al-Cu-Mg-Ag alloys with low-ratios of Cu/Mg, i.e., Al-4.9Cu-0.8Mg-1.1Ag-0.3Mn-0.15Zr (wt.%) alloy [45] and Al-5.1Cu-1.0Mg-0.6Ag (wt.%) alloy [46],

the size and quantity of the Ω phase (Al_2Cu with Mg and Ag segregated at the Ω interface) have been the main focus, but the role of the S phase (Al_2CuMg) in the mechanical properties has been largely ignored. The detailed strengthening effects and the competitive relationships of consumption of Cu and Mg by both the Ω phase and the S phase should be further investigated. In the present work, an attempt was to further elucidate the strengthening effects of the Ω phase and the S phase in Al-5.1Cu-1.0Mg-(0.4Ag) (wt.%) aluminum alloys with a low Cu/Mg ratio (Cu/Mg ratio: 5.1), thereby studying the corresponding microstructural evolutions and their correlations with the mechanical properties. To explore the effects of Ag addition on the evolution of the Ω and S phases, detailed characterizations were conducted by (scanning) transmission electron microscopy, (S)TEM, to analyze the sizes and morphologies of both precipitates in the under-aged, peak-aged, over-aged, and prolonged ageing conditions.

2. Experimental procedure

Two Al-Cu-Mg aluminum alloys with the same basic composition of Al-5.1Cu-1.0Mg (wt.%) but different Ag concentrations of 0 and 0.4 (wt.%), designated as Alloy 0A and Alloy 4A, respectively, were investigated in this work. The two samples were prepared by vacuum induction melting, and the purity of each constituent element was at least 99.9% (weight percent, wt%); their chemical compositions, listed in Table 2, were measured by arc spark optical emission spectroscopy on SPECTROMAXx (SPECTRO-AMETEK Inc., PA, USA). The as-

cast ingots were first homogenized at 515 °C for two days, followed by hot rolling at 450 °C to produce 3 mm thick sheets with an 85 % reduction in thickness. After solution treatment at 515 °C for 2 h, the specimens were water quenched and then naturally aged for 4 days. Subsequently, artificial ageing treatments were conducted at 185 °C for different holding times ranging from 1 to 100 h. Vickers hardness tests for the related samples were performed with a 500g load for 8 s by using a Vickers hardness tester, FM-700 (Future-Tech Corp, Tokyo, Japan). The hardness test specimens were prepared by grinding with 800# to 4000# SiC sandpaper to eliminate scratches on the surfaces of the samples, and each average value of hardness data with the corresponding standard deviation was obtained from at least 30 measurements of the same specimen. The peak ageing state (aged at 185 °C for 11 h), denoted as T6, and the over ageing state (aged at 185 °C for 18 h), denoted as T7, were determined from the artificial age-hardening curve. Specimens aged at 185 °C for 5 h and 100 h were also investigated to understand the precipitate evolution in these two alloys. The tensile tests of the 5 h, 11 h (T6), 18 h (T7), and 100 h ageing treated samples of both Alloy 0A and Alloy 4A were performed with the MTS Landmark 370.02 Dynamic Test System (MTS Systems Corporation, Eden Prairie, MN, USA) at a strain rate of 10^{-3} s^{-1}. The tensile test specimens were prepared according to the standard of ASTM B557M-15. The TEM specimens were sliced from the relevant ageing treated samples, thinned to 0.07 mm and then electropolished by a twin-jet polisher at –30 °C with a mixture of 33% nitric acid and 67% methanol until perforation. They were examined on a Tecnai G2 F30

(Thermo Fisher Scientific, Waltham, MA, USA) with a double tilt stage and operated at 300 kV to investigate the evolution of the Ω and S phases. In addition, the crystallography of Ω and S phases was analyzed by using high-resolution (S)TEM images with fast Fourier transformation (FFT) diffractograms, which were collected on a JEOL ARM200F (JEOL, Tokyo, Japan) with a Cs-corrector operated at 200 kV. For measurement of the diameter (i.e., the platelet length of the Ω phase in edge-on configuration, also denoted as the size) and volume percent of the Ω phase, the $[110]_{Al}$ zone axis was chosen to observe edge-on configurations of the Ω phase variants. For each ageing treatment, the Ω phase was measured on more than 1000 precipitates in four different aluminum grains observed in the TEM images. According to the previous works [17, 21], the volume percent (V) of the Ω phase was estimated as $V = W \times \sum_{i=1}^{N} v_i$. In the formula $v_i = d^2\pi t/4$, the morphology of Ω phase is assumed to be disk-shaped, and t the thickness of the Ω phase and d, the diameter. In addition, a correction factor [17, 21] is considered and expressed as $W = [1+ (f +\bar{d})/\sqrt{A}] / [A (f + \bar{d})]$, where $\bar{d}$ is the average disk diameter of Ω phase, f is the thin foil thickness, and A is the observed area of the TEM image. The need for a correction factor for the measurement was due to the large diameter of the Ω phase, which had probably extended beyond the surface of the thin foil, as shown in Fig. 1. In addition, due to half of non-edge-on variants of the Ω phase could not be observed in TEM image, $V =2\times W\times \sum_{i=1}^{N} v_i$ was considered. The TEM thin foil thickness, f, was determined by the log-ratio method [65] of electron energy loss spectroscopy (EELS). The mean free path of

aluminum used 124 nm here for calculation [65] and the collection of EELS spectra was performed on the Tecnai G2 F30 TEM in TEM mode with a semi-collection angle of ~19.4 mrad [66].

Table 2. Chemical compositions (in wt. %) of Al-Cu-Mg-(Ag) alloys studied.

Two Alloys	Cu	Mg	Ag	Mn	Zr	Ti	Zn	Al
Alloy 0A	5.11	0.96	-	0.59	0.13	0.06	0.01	Bal.
Alloy 4A	5.13	0.97	0.38	0.57	0.11	0.06	0.01	Bal.

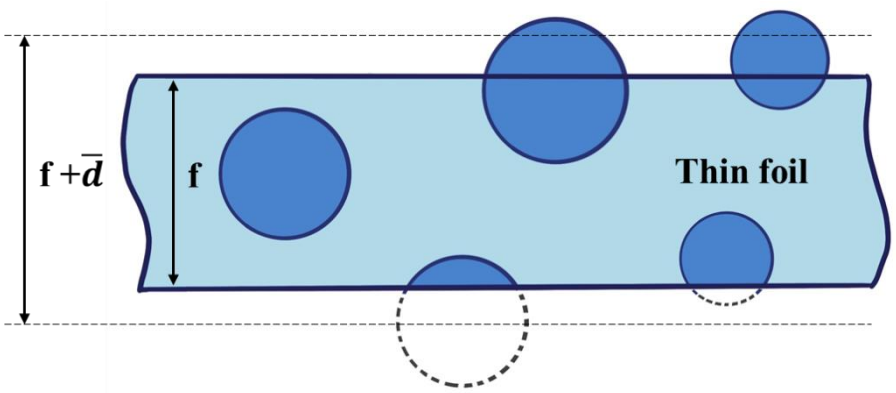


Fig. 1. The illustration of the Ω phase distribution within and extending beyond the aluminum thin foil.

3. Results

3.1. Mechanical properties

Fig. 2 shows the Vickers hardness (HV) as a function of artificial ageing time for the specimens of Alloy 0A and Alloy 4A aged at 185 °C for different holding times ranging from 1 to 100 h. At the initial ageing stage in the first hour (1 h), the hardness of Alloy 4A specimen increased rapidly compared with that of Alloy 0A; the former increased from 96.4 ± 2.2 to 121.4 ± 2.9 HV (~26 %), and the latter, from 93.5 ± 1.9 to 105.7 ± 2.3 HV (~13 %). As the ageing

continued, the hardness of both specimens increased and reached the maximum hardness (i.e., peak ageing) as the ageing was conducted at 185 °C for 11 h (i.e., the T6 treatment). The hardness of Alloy 4A (165.9 ± 3.1 HV) was about 19.8 % higher than that of Alloy 0A (138.5 ± 2.8 HV). After the peak ageing stage, the hardness of both specimens gradually decreased. Ageing at 185 °C for 18 h was chosen in the present work to perform as the T7 treatment; the purpose of this over ageing treatment [67, 68] has been asserted to enhance the stability of precipitates, total elongation and intergranular corrosion (IGC) resistance, although it brings about a slightly lower strength. After the T7 treatment, the hardness of both Alloys 0A and 4A declined; the former was 127.6 ± 1.7 HV, while the latter was 151.1 ± 2.3 HV. In Fig. 2, the precipitation hardening curves display that during prolonged ageing up to 100 h, the hardness of Alloy 0A specimens slowly decreased, while that of Alloy 4A specimens remained nearly constant. The curves show that the specimen of Alloy 0A aged for 5 h had approximately the same hardness as that aged for 18 h, and the specimen of Alloy 4A also had the same trend. In the present work, both Alloys 0A and 4A samples respectively aged at 185°C for 5 h, 11 h (T6), 18 h (T7) and 100 h were examined to explore the structure–property relationships; the difference in hardness for the samples of Alloy 4A treated with four different ageing times and their counterparts, Alloy 0A, is illustrated by the elongated frames in Fig. 2. Hereafter, the corresponding samples for Alloy 0A are labelled as 0A-5h, 0A-11h (i.e., 0A-T6), 0A-18h (i.e., 0A-T7) and 0A-100h; the corresponding samples for Alloy 4A are denoted as 4A-5h, 4A-11h

(i.e., 4A-T6), 4A-18h (i.e., 4A-T7) and 4A-100h. Table 3 presents the data of tensile tests for Alloy 0A and 4A specimens. Consistent with the results of the hardness tests (Fig. 2), the ultimate tensile strength (UTS) of the 4A-5h specimen was much higher than that of the 0A-5h specimen; the former was 495 MPa (with 16.4% total elongation), whereas the latter was 401 MPa (with 16.5% total elongation). For the T6 ageing treatment, both the 4A-T6 specimen (530 MPa) and the 0A-T6 (456 MPa) specimen reached their highest UTSs, but their total elongation decreased to 10.2 % and 12.5 %, respectively. As to the T7 treatment, the UTS of the 4A-T7 specimen slightly decreased to 511 MPa (–3.5 % as compared with 4A-T6), while that of the 0A-T7 specimen dropped to 412 MPa (–9.6 % as compared with 0A-T6). With prolonged ageing treatment, the 4A-100h specimen still maintained a high UTS (449 MPa) as compared with that of the 0A-100h specimen (326 MPa). The microstructural evolution for ageing at 5 h, 11 h, 18 h, and 100 h in Alloys 0A and 4A will be presented in the following sections.

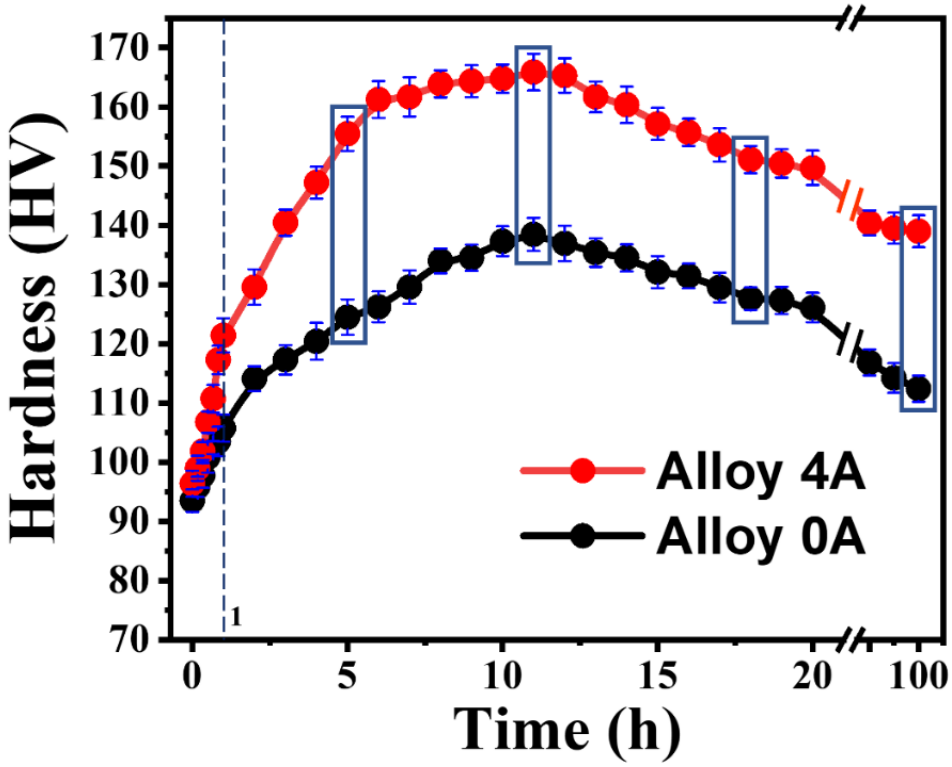


Fig. 2. Age-hardening curves of Ag-free (Alloy 0A) and Ag-containing (Alloy 4A) samples aged at 185 °C for different holding times from 0 to 100 h.

Table 3 YSs, UTSs, Els, and comparison of UTSs (based on T6 condition) of Alloys 0A and 4A aged at 185 °C for 5, 11 (T6), 18 (T7), and 100 h.

Sample	Alloy 0A				Alloy 4A			
	YS (MPa)	UTS (MPa)	EL (%)	UTS difference	YS (MPa)	UTS (MPa)	EL (%)	UTS difference
5 h	310 ± 5	401 ± 10	16.5 ± 0.3	-12.1 %	410 ± 6	495 ± 9	16.4 ± 0.9	-6.6 %
11 h (T6)	372 ± 7	456 ± 9	12.5 ± 0.4	0 %	473 ± 11	530 ± 12	10.2 ± 0.3	0 %
18 h (T7)	350 ± 6	412 ± 7	14.2 ± 0.4	-9.6 %	442 ± 10	511 ± 11	12.6 ± 0.2	-3.5 %
100 h	298 ± 3	326 ± 8	10.4 ± 0.2	-28.5 %	395 ± 11	449 ± 9	10.9 ± 0.4	-15.3 %

YS: Yield strength; UTS: Ultimate tensile strength; EL: Total elongation

3.2. TEM Analysis of Alloy 0A

Figs. 3a-c show TEM images and selected area diffraction (SAD) patterns along the $[001]_{Al}$ zone axis for Alloy 0A specimens aged at 185 °C for 5 h, 11 h (T6) and 18 h (T7), i.e., 0A-5h, 0A-T6 and 0A-T7 accordingly. At the early stage of artificial ageing at 185 °C for 5 h,

the S phase preferred to nucleate on dislocations and around the T phase interfaces (as indicated by arrows in Fig. 3a), which were prone to be the easy nucleation sites due to the loci of stress concentration; the red arrows refer to the S phase with edge-on configuration, while the purple arrows denote the T phase, whose boundaries were surrounded by the S phase. Under 5 h ageing treatment for Alloy 0A, the amounts of S phase were still too low to contribute to diffraction spots in the selected area diffraction (SAD) patterns, as shown in the inset of Fig. 3a. After ageing for 11 h, the peak ageing stage (T6) was achieved in Alloy 0A; the edge-on configuration S phase on the dislocations increased in both size and number, and their diffraction patterns are very faint but still discerned, as indicated by red spots in the inset of Fig. 3b. The same diffraction spots can be seen in Fig. 3c obtained from Alloy 0A specimen aged at 185 °C for 18 h (T7). It is worth noting that, under observation along the axis of the $[001]_{Al}$ zone, in addition to the 4 S-phase with edge-on configurations, the other 8 S-phase with non-edge configurations projected as 2 perpendicular variants, which were characterized by elongated bundle-like layers parallel to the $[100]_{Al}$ and $[010]_{Al}$ directions, as shown in Fig. 3b-d (indicated by the green arrows). A More detailed illustration of S phase images can be seen in Section 3.3. It should be noted that, under a specific zone axis observation, the correlation between habit plane and growth direction of all S phase variants should be properly examined. The orientation relationships of all 12 variants of S phase with aluminum matrix are listed in Table 4, and their intersection directions on the $(001)_{Al}$ plane are also listed in Table 5. Among them, 4 (variants

1-4) of 12 variants show edge-on configurations while other 8 variants (variants 5-12) display non-edge on configurations when observing along $[001]_{Al}$ zone axis. In the edge-on configuration (variants 1-4) in a two-dimensional TEM imaging plane, the projected images of these precipitates are along $[210]_{Al}$, $[2\bar{1}0]_{Al}$, $[120]_{Al}$, and $[\bar{1}20]_{Al}$, respectively. On the other hand, both variants 5-8 and variants 9-12 (in Table 5) of S phase possess the intersection directions along $[010]_{Al}$ and $[100]_{Al}$ directions on $(001)_{Al}$ plane. However, the images of variants 5-8 on $(001)_{Al}$ plane along $[010]_{Al}/[100]_{Al}$ cannot be distinguished with each other under this observation along $[001]_{Al}$ zone axis; nor can those of variants 9-12. After ageing for 18 h, a considerable number of edge-on configurations S phase and non-edge-on configuration S phase (denoted as S bundles) dominated in the aluminum matrix, with the corresponding diffraction spots becoming brighter, as shown in the inset of Fig. 3c. The STEM image in Fig. 3d for an Alloy 0A sample aged at 185°C for 100 h clearly shows that the rather dark lump-shaped T phase was surrounded by the S phase (with higher Z-contrast), which was located at the bright borders, and that the aluminum matrix was abundant in S bundles. Previous works [58, 59, 69] have been proposed that the S phase forms on the $\{012\}_{Al}$ habit planes and grows along the $<1\ 0\ 0>_{Al}$ directions. The STEM study in the present work (Fig. 3d) also clearly shows the S phase with non-edge-on configuration (denoted as S bundles, indicated by green arrows) elongated along $[1\ 0\ 0]_{Al}$ and $[0\ 1\ 0]_{Al}$ directions; whereas the S phase with edge-on configuration exhibits a line-like morphology (denoted as S, indicated by red arrows),

suggested to be elongated along the zone axis $[0\ 0\ 1]_{Al}$ direction. Observation of the evolutions of the S phase and the S bundles in the samples aged at 185°C from 5 h to 100 h at a higher magnification will be reported in Sections 3.5 and 3.6.

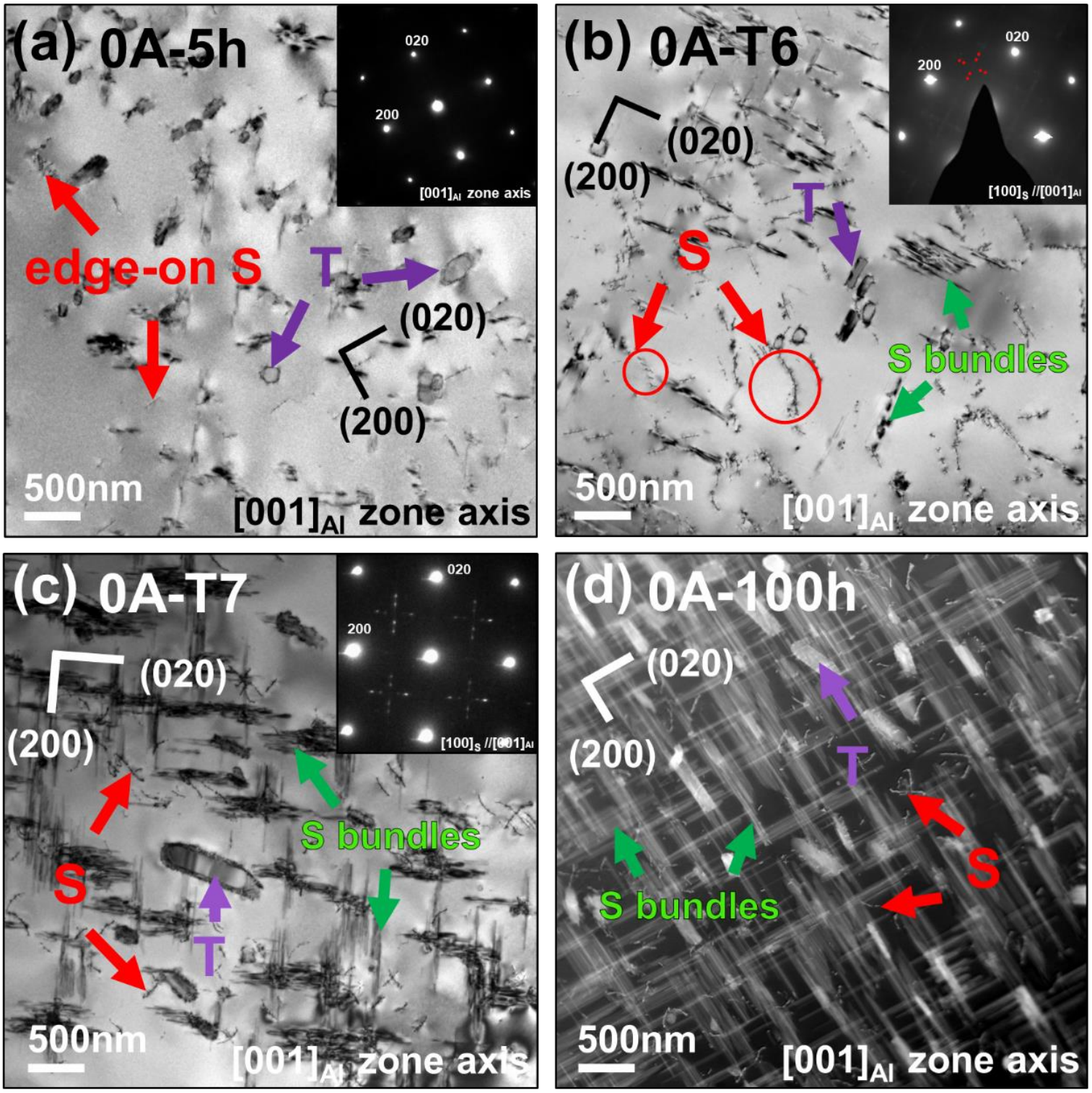


Fig. 3. TEM images of the morphologies of nano-precipitates and their diffraction patterns observed along the $[001]_{Al}$ zone axis in Alloy 0A specimens aged for (a) 5 h, (b) 11 h (T6) and (c) 18 h (T7); STEM image observed along the $[001]_{Al}$ zone axis for (d) 100 h. The red arrows refer to the S phase with edge-on configuration, while the green arrows, the S phase with non-edge-on configuration (denoted as S bundles). Some brighter particles in (d) due to the T phase overlapping with the S phase.

Table 4. Orientation relationships between S phase variants and aluminum matrix.

Variant	Parallel plane	Parallel direction
Variant 1	$(001)_S$ //$(\bar{1}20)_{Al}$	$[010]_S$ // $[210]_{Al}$
Variant 2	$(001)_S$ // $(120]_{Al}$	$[010]_S$ // $[2\bar{1}0]_{Al}$
Variant 3	$(001)_S$ // $(\bar{2}10)_{Al}$	$[010]_S$ // $[120]_{Al}$
Variant 4	$(001)_S$ // $(\bar{2}\bar{1}0)_{Al}$	$[010]_S$ // $[\bar{1}20]_{Al}$
Variant 5	$(001)_S$ // $(0\bar{2}1)_{Al}$	$[010]_S$ // $[012]_{Al}$
Variant 6	$(001)_S$ // $(0\bar{2}\bar{1}))_{Al}$	$[010]_S$ // $[0\bar{1}2]_{Al}$
Variant 7	$(001)_S$ // $(0\bar{1}2)_{Al}$	$[010]_S$ // $[021]_{Al}$
Variant 8	$(001)_S$ // $(012)_{Al}$	$[010]_S$ // $[02\bar{1}]_{Al}$
Variant 9	$(001)_S$ // $(20\bar{1})_{Al}$	$[010]_S$ // $[102]_{Al}$
Variant 10	$(001)_S$ // $(201)_{Al}$	$[010]_S$ // $[\bar{1}02]_{Al}$
Variant 11	$(001)_S$ // $(10\bar{2})_{Al}$	$[010]_S$ // $[201]_{Al}$
Variant 12	$(001)_S$ // $(\bar{1}0\bar{2})_{Al}$	$[010]_S$ // $[20\bar{1}]_{Al}$

Table 5. The intersection directions between 12 variants of S phase and the observation plane $(001)_{Al}$.

Variant	Intersection direction
Variant 1	$(\bar{1}20)_{Al}$
Variant 2	$(120]_{Al}$
Variant 3	$(\bar{2}10)_{Al}$
Variant 4	$(\bar{2}\bar{1}0)_{Al}$
Variant 5	$[\bar{1}00]_{Al}$
Variant 6	$[100]_{Al}$
Variant 7	$[\bar{1}00]_{Al}$
Variant 8	$[100]_{Al}$
Variant 9	$[0\bar{1}0]_{Al}$
Variant 10	$[010]_{Al}$
Variant 11	$[0\bar{1}0]_{Al}$
Variant 12	$[010]_{Al}$

3.3. Analysis of 12 variants of S phase

In Al-Cu-Mg aluminum alloys with low Cu/Mg ratios, such as the alloys investigated in the present work, the S phase precipitates are expected to be the main strengthening precipitates

[5, 7-10]. While their edge-on configuration structure has been extensively studied [7, 10, 61, 62, 69], the projected images of their non-edge-on configuration on the $(001)_{Al}$ plane in TEM observation has seldom been reported in previous works [54, 69] and need to be further elucidated. Here, in Fig. 4a, a HAADF STEM image taken from an Alloy 4A sample aged at 185 °C for 100 h displays the edge-on and non-edge-on configurations of S phase precipitates observed along the $[001]_{Al}$ zone axis. The red dotted square in Fig. 4a is enlarged in Fig. 4b, where four edge-on configuration S phase variants growing on $\{120\}_{Al}$ habit planes, namely variant 1: $(\bar{1}20)_{Al}$, variant 2: $(120)_{Al}$, variant 3: $(2\bar{1}0)_{Al}$ and variant 4: $(210)_{Al}$, are indicated by red arrows. Figs. 4c-f present EDS mapping images to complement the Z-contrast HAAF-STEM image in Fig. 4a. The projected images of lath-like S phase precipitates (Al_2CuMg) with non-edge-on configuration are elongated along the $[100]_{Al}$ and $[010]_{Al}$ directions and appear as a bundle-like morphology (indicated by green arrows in Fig. 4a) on the $(001)_{Al}$ projection plane. The existence of Mg in these bundles, as shown in Fig. 4c, is strong evidence for their identification as the non-edge-on S phase precipitates (Al_2CuMg) rather than the edge-on θ' phase (Al_2Cu). Observed along $[001]_{Al}$ zone axis, the morphology of edge-on configuration θ' phase precipitate, whose habit plane is the $\{001\}_{Al}$ plane [6], is similar to that of the non-edge-on configuration S phase. As a result, the TEM observations along this zone axis in the current work may cause confusion.

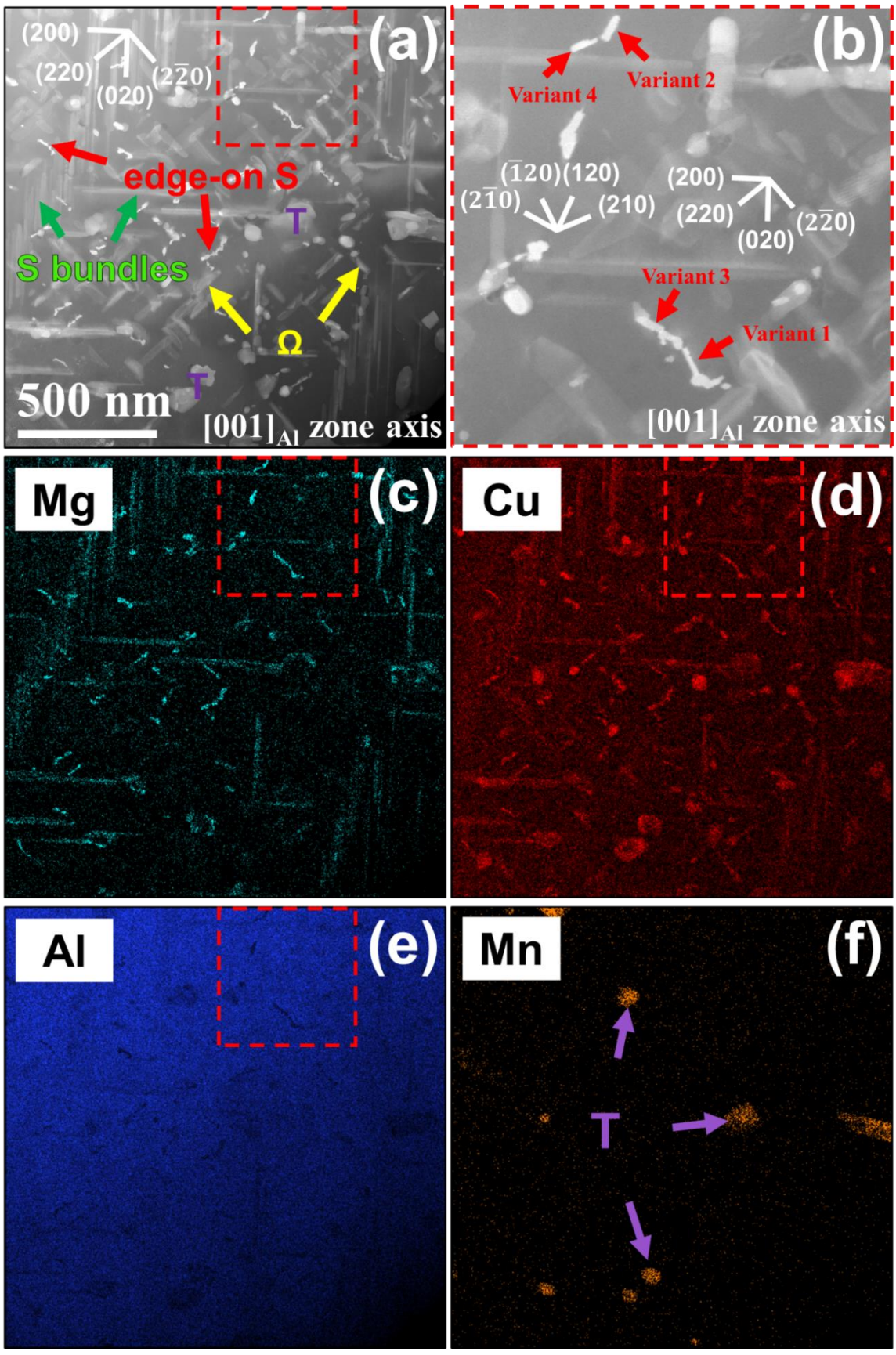


Fig. 4. (a) A HAADF-STEM image of the sample 4A-100h observed along the $[001]_{Al}$ zone axis, (b) an enlarged image from red dotted square in (a), and the corresponding EDS mapping images of (c) Mg, (d) Cu, (e) Al and (f) Mn elements. T phase indicated by T in (f), rich in Mn.

3.4. TEM Analysis of Alloy 4A

Figs. 5a-c present TEM images observed along the $[110]_{Al}$ zone axis with the corresponding selected area diffraction (SAD) patterns for Alloy 4A specimens aged at 185 °C for 5 h, 11 h (T6) and 18 h (T7), i.e., 4A-5h, 4A-T6 and 4A-T7 accordingly. Although a previous work [9] indicated that the Ω phase existed as 12 variants, some other works [37, 69, 70] considered it only 4 variants. Actually, in the view point of crystallography, each of four $\{111\}_{Al}$ plane possesses three variants of the Ω phase growing along three $<110>_{Al}$ directions, as shown in Table 1, thus 12 variants. However, viewing along the $[110]_{Al}$ zone axis, since the Ω phase grows in a disk-like morphology, it is impossible to distinguish the three variants of the Ω phase on each $\{\bar{1}11\}_{Al}$ habit plane, so the Ω phase is generally considered to be 4 variants, associated with 4 different habit planes. Under the observation of $[110]_{Al}$ zone axis, two of four variants in the edge-on configuration on two habit planes, $(\bar{1}11)_{Al}$ and $(1\bar{1}1)_{Al}$, can be identified to have a line-like morphology (indicated by yellow arrows), inclined at an angle of 70.52° to each other, as shown in Figs. 5a-c. Fig. 5a shows numerous and tiny Ω phase uniformly distributed in the aluminum matrix of an Alloy 4A sample aged at 185 °C for 5 h, while the S phase can barely be observed. The ultrathin edge-on disk-shaped Ω phase growing on the $\{111\}_{Al}$ plane resulted in only blurred streaks in diffraction patterns along the $\bar{1}11_{Al}$ and $1\bar{1}1_{Al}$ poles, indicated by yellow arrows in the inset of diffraction patterns of Figs. 5a. After the 11 h (T6) ageing treatment, the Ω variants became denser with a larger aspect ratio (Fig. 5b). In addition to the

stronger streaks, two faint diffraction spots at $\frac{1}{3}\ \bar{2}20_{Al}$ and $\frac{2}{3}\ \bar{2}20_{Al}$ can be identified as being associated with the other two non-edge-on variants of Ω phase, as indicated by white arrows in the insets of the diffraction patterns in Figs. 5b and c. After ageing for 18 h (T7), the average diameter of the Ω phase grew further and the aspect ratio continued to increase, while the spacings between them became wider, as shown in Fig. 5c. After ageing for 100 h, the distribution of the Ω phase was still uniform, as shown in the STEM image in Fig. 5d. The line-like Ω phase (with edge-on configurations) in the samples aged at 185 °C for different holding times indicates that the Ω phase had high thermal stability at this temperature throughout different holding periods. In addition to the Ω phase, S phase was also observed. As shown in Figs. 5b and c under the observation of [110] zone axis, the S phase appeared to have a parallel-striped morphology (indicated by green arrows) along the $[\bar{1}10]_{Al}$ direction, and its surrounding strain field caused blurring in the image. The STEM image in Fig. 5d also shows the same characteristic of the S bundles under observation along the $[110]_{Al}$ zone axis, revealing that a considerable amount of S phase existed. Figs. 5e and f present the data of the average size and the volume percent of the Ω phase in Alloy 4A aged at 185 °C for different holding times. In the specimen treated for 5 h, the average size (the length of the line-like Ω phase, also denoted as diameter) and the volume percent of the Ω phase were estimated to be 23 nm and 0.29 vol. %, respectively. In the T6 treatment, the Ω phase grew to an average diameter of 76 nm and the volume percent reached the highest value, 4.23 vol. %. In the T7 treatment, with much longer-

time treatment, the Ω phase continually increased to 127 nm, whereas the volume percent decreased slightly to 3.82 vol. %. After prolonged holding at 185 °C for 100 h, the average diameter further grew to 257 nm, while the volume percent dropped somewhat to 2.74 vol. %.

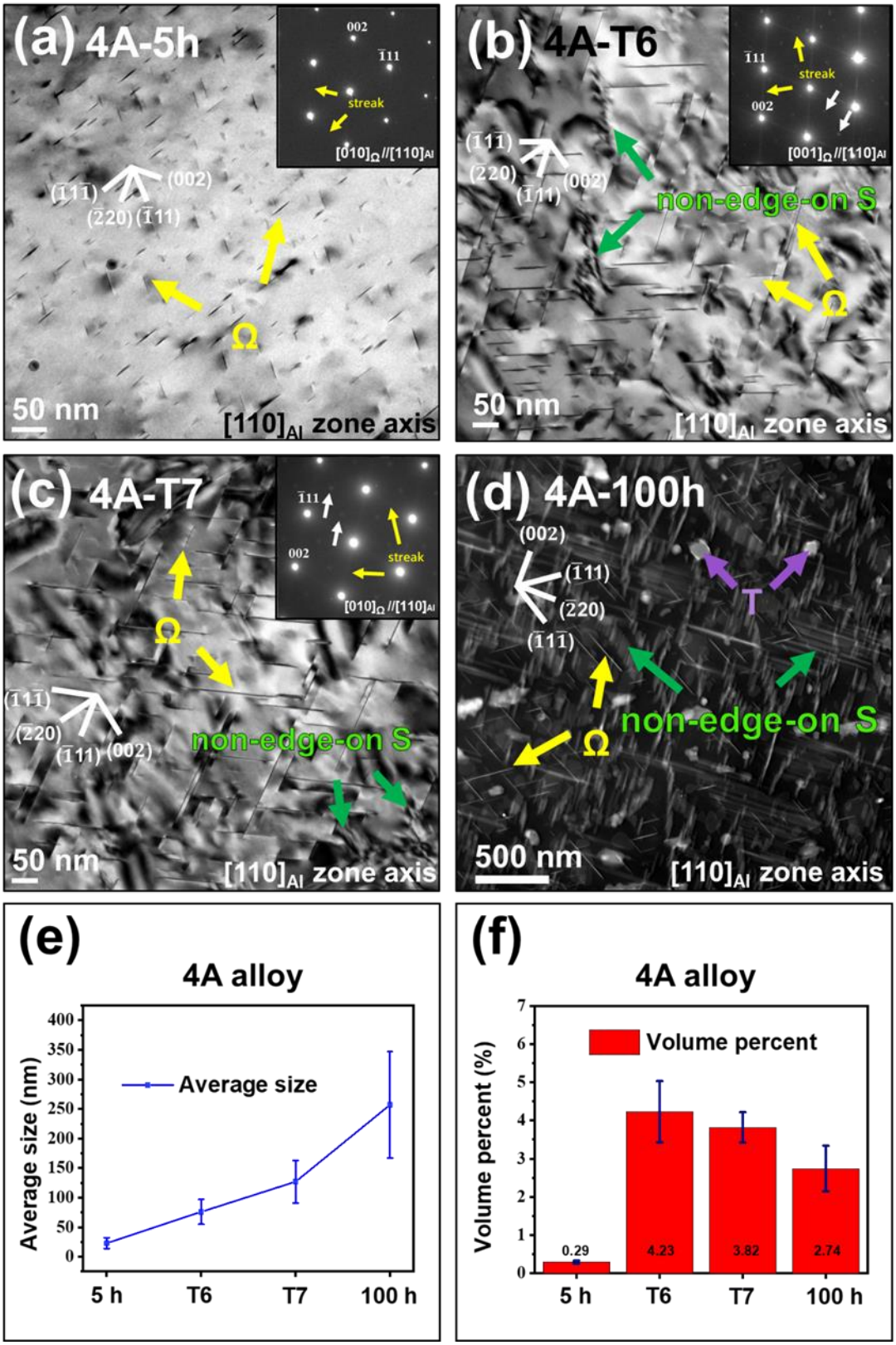


Fig. 5. Morphologies of nano-precipitates observed along the $[110]_{Al}$ zone axis in Alloy 4A specimens. TEM images and the corresponding diffraction patterns for Alloy 4A samples aged at 185 °C for (a) 5 h, (b) 11 h (T6), and (c) 18 h (T7). (d) STEM image of Alloy 4A specimen aged at 185 °C for 100 h. Plots (e, f) of average size and volume percent of the Ω phase versus ageing time (5 h, 11 h, 18 h, and 100 h).

3.5. TEM Analysis of S phase

To clearly reveal the evolution of the S phase in Alloys 0A and 4A samples respectively treated at 185 °C for 5, 11, 18, and 100 h, the zone axis was slightly deviated from $[001]_{Al}$ to bring about a bright-contrast aluminum matrix in the corresponding TEM images. TEM images of Alloy 0A specimens are shown in Figs. 6a-d, and those of Alloy 4A specimens, in Figs. 6e-h. The black particles in Figs. 6a-d are the S phase growing on the $\{120\}_{Al}$ plane, and edge-on configuration variants can be clearly observed along this axis as illustrated in Table 4. Two mutually perpendicular variants of the S bundles (with gray contrast) elongated along the $[100]_{Al}$ and $[010]_{Al}$ directions can be observed in Figs. 6b-d and f-h. In the 0A-5h specimen, the densely-distributed tiny S phase were observed to have formed on the dislocations, as shown in Fig. 6a. After ageing for 11 h, the dislocations were fully decorated by the S phase, and two perpendicular variants of the S bundles were observed, as shown in Fig. 6b. Figs 6c and d, which were taken from 0A specimens aged respectively for 18 h and 100 h, display that the coarsened S phase coalesced and the S bundles grew. Figs. 6e-h present TEM images of Alloy 4A specimens aged for 5, 11, 18 and 100 h, and the S phase (with edge-on configuration) and the S bundles (with non-edge-on configuration) are also visible. The greatest difference between Alloys 0A and 4A was the formation of uniform Ω phase in the aluminum matrix in Alloy 4A specimens; i.e., the Ω phase was found only in Alloy 4A specimens. Under observation of the near [001] zone axis, the Ω phase was not in the edge-on configuration and appeared as gray-

colored lath-like particles, as indicated by yellow circles, densely distributed (Figs. 6e-h). It should be noted that, under observation of the $[001]_{Al}$ zone axis, the projection of four variants of the Ω phase with the $\{111\}_{Al}$ habit plane just displayed two perpendicular variants along the [110] and $[1\bar{1}0]$ directions; in addition, the sizes of the Ω phase in Figs. 6e-h were respectively consistent with those edge-on configurations in Figs. 5a-d. In the 4A-5h specimen (Fig. 6e), besides the Ω phase, a few S phase growing on dislocations were seen. Comparison of the microstructures in the 4A-T6 (Fig. 6f) and 0A-T6 specimens (Fig. 6b) revealed that there were no significant differences in the sizes of the S phase and S bundles except for the formation of the densely-distributed Ω phase in the 4A-T6 specimen (Fig. 6f). After further ageing for 18 h, the S phase and S bundles in the 4A-T7 specimen (Fig. 6g) were similar in size to those in the 4A-T6 specimen (Fig. 6f); however, the same treatment condition brought about much larger S phase and S bundles in the 0A-T7 specimen (fig. 6c), as compared with those in the 4A-T7 (Fig. 6g). In the 100 h treated specimen of the Alloy 4A, the S phase coalesced, as shown in Fig. 6h, reaching a size approximately the same as that of the 0A-100h specimen (Fig. 6d).

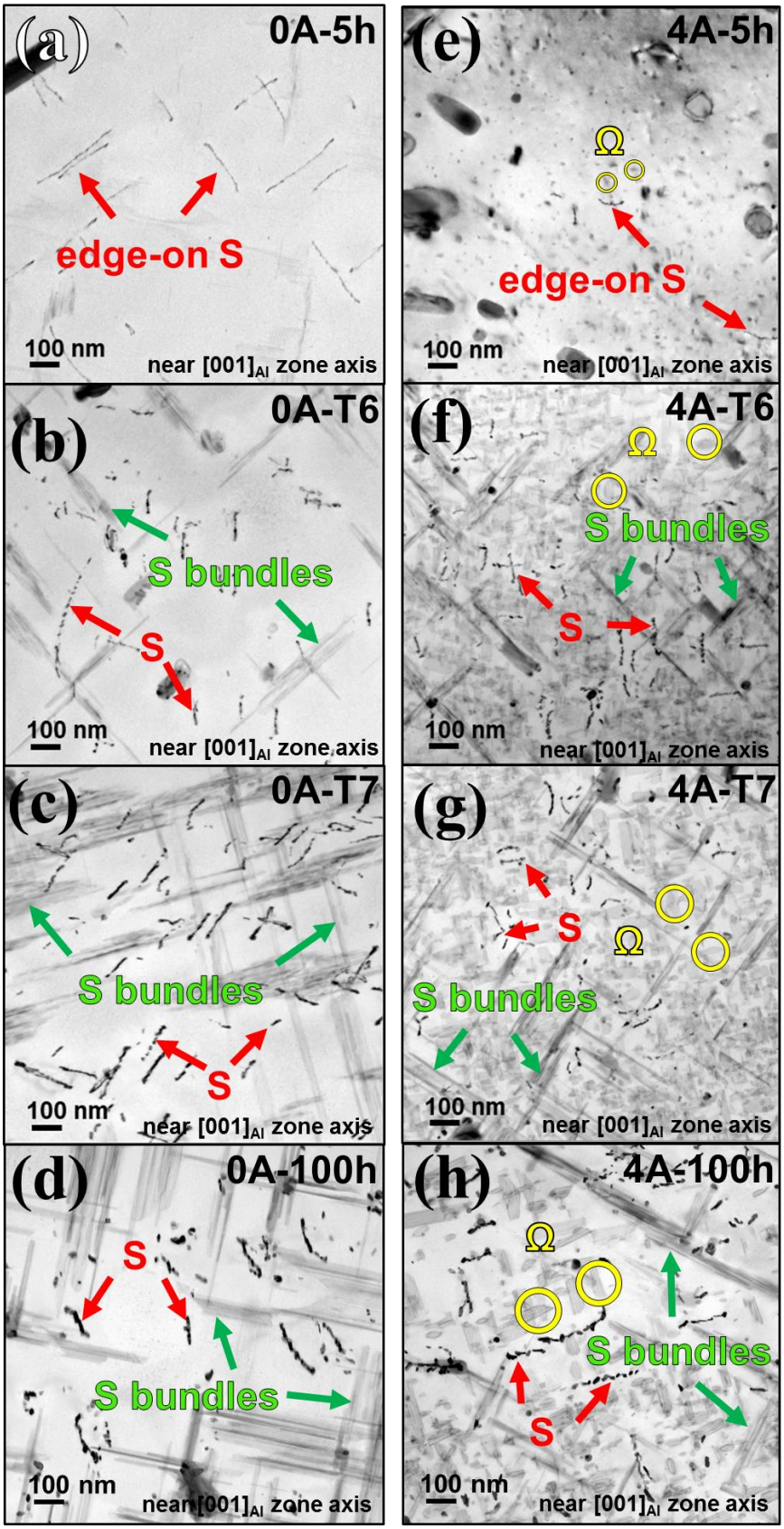


Fig. 6. TEM images of nano-precipitate morphologies observed near the $[001]_{Al}$ zone axis in Alloy 0A specimens: (a) 5 h, (b) T6, (c) T7, (d) 100h; and Alloy 4A specimens: (e) 5 h, (f) T6, (g) T7, and (h) 100h. The edge-on S phase (denoted as S) indicated by the red arrows, while the non-edge-on S phase (denoted as S bundles), the green arrows.

3.6. HR-(S)TEM crystallographic Analysis

The detailed morphologies and crystallographic structures of the S phase and Ω phase are presented in this section. The striking morphology of the S phase has been observed by HR-TEM, as shown in Fig. 7. Two edge-on configuration variants forming on $(1\bar{2}0)_{Al}$ and $(2\bar{1}0)_{Al}$ in Fig. 7a are connected to each other (in a zigzag form) on one dislocation with a specific angle of 36.87° (or 143.13 °) as observed along the $[001]_{Al}$ zone axis in the 0A-T6 specimen. These two variants were clearly identified by the corresponding fast Fourier transformation (FFT) diffractograms (indicated by the solid and dashed frames on the right side of Fig. 7a) and simulated diffraction patterns. In contrast, an HR-TEM image taken from the over-aged 0A-T7 specimen (Fig. 7b) shows that three precipitates of S phase with the same orientation (i.e., the same variant) were joined together, with the coarser one displaying the distinctive ledge characteristic. The S phase in 0A-T6 specimen (Fig. 7a) possesses a sharp boundary, while the coarsened S phase in 0A-T7 specimen (Fig. 7b), indicated by the red arrows, has a ledge boundary. The former has been identified in the previous works as meta-stable SI, and the latter, as equilibrium SII [61, 62]. Fig. 8a presents the representative HR-STEM image of the Ω phase whose thickness remained around 3 nm when Alloy 4A was treated at 185 °C for 100 h, indicating the high thermal stability of its thickness. The HR-STEM image of Fig. 8a was only filtered by excluding the FFT outside the gray circle in Fig. 8b, and no other image processing was performed. The brighter z-contrast at the interface between the Ω phase and aluminum

matrix are presumed to be the segregation of Ag atoms, which possess a higher atomic number. The atomic distribution of the Ω phase illustrating in Fig. 8c was referred to the previous work [28] on Al-6.4Cu-0.45Mg-0.4Ag-0.3Mn-0.15Zr alloy. The consistence of atomic distribution with the z-contrast image in Fig 8a further confirmed the segregated Ag at the interface of the Ω phase and aluminum matrix.

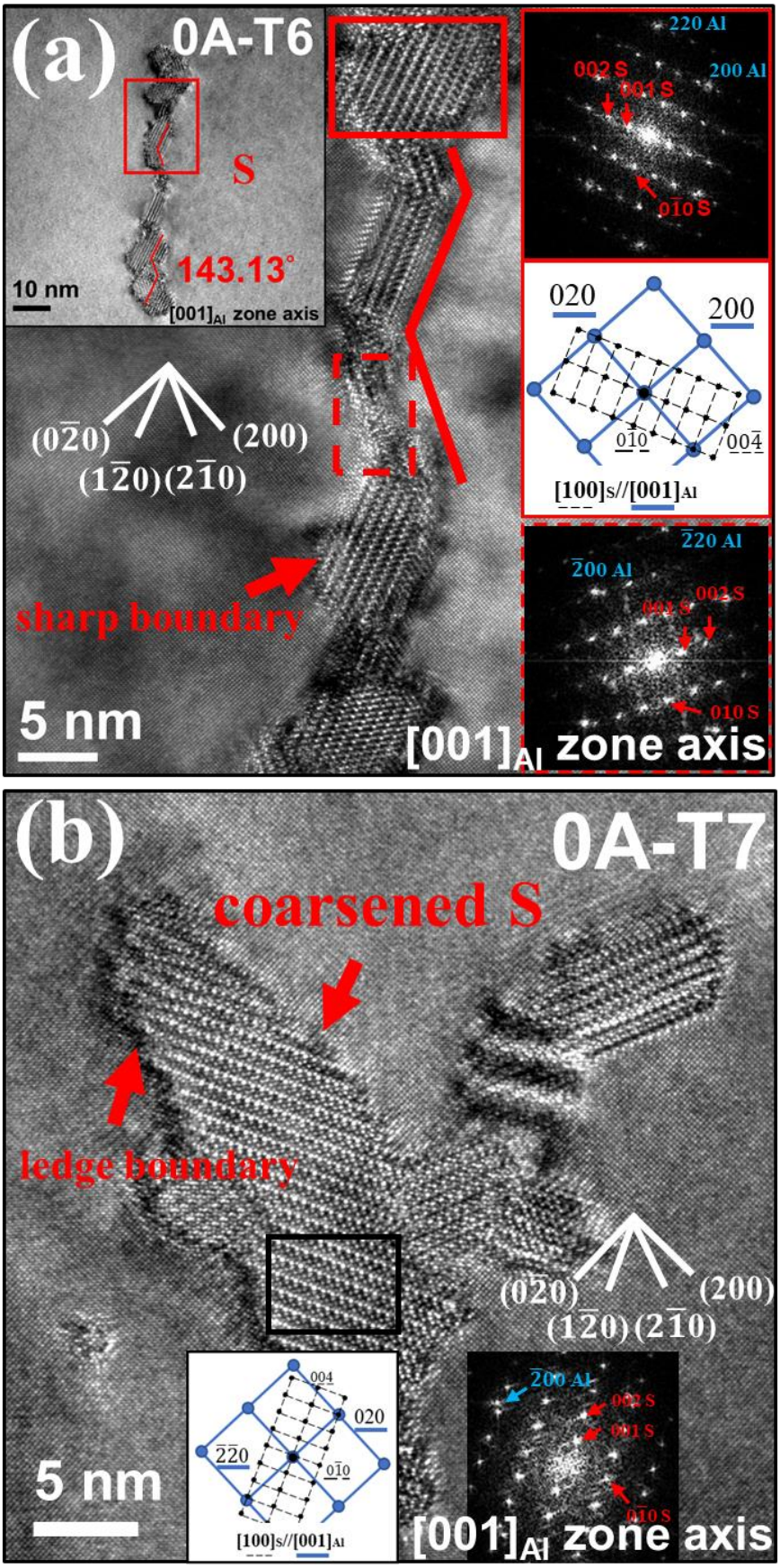


Fig. 7. HR-TEM images of the S phase with corresponding FFT diffractograms and simulated diffraction patterns observed along the $[001]_{Al}$ zone axis in (a) 0A-T6 and (b) 0A-T7 specimens.

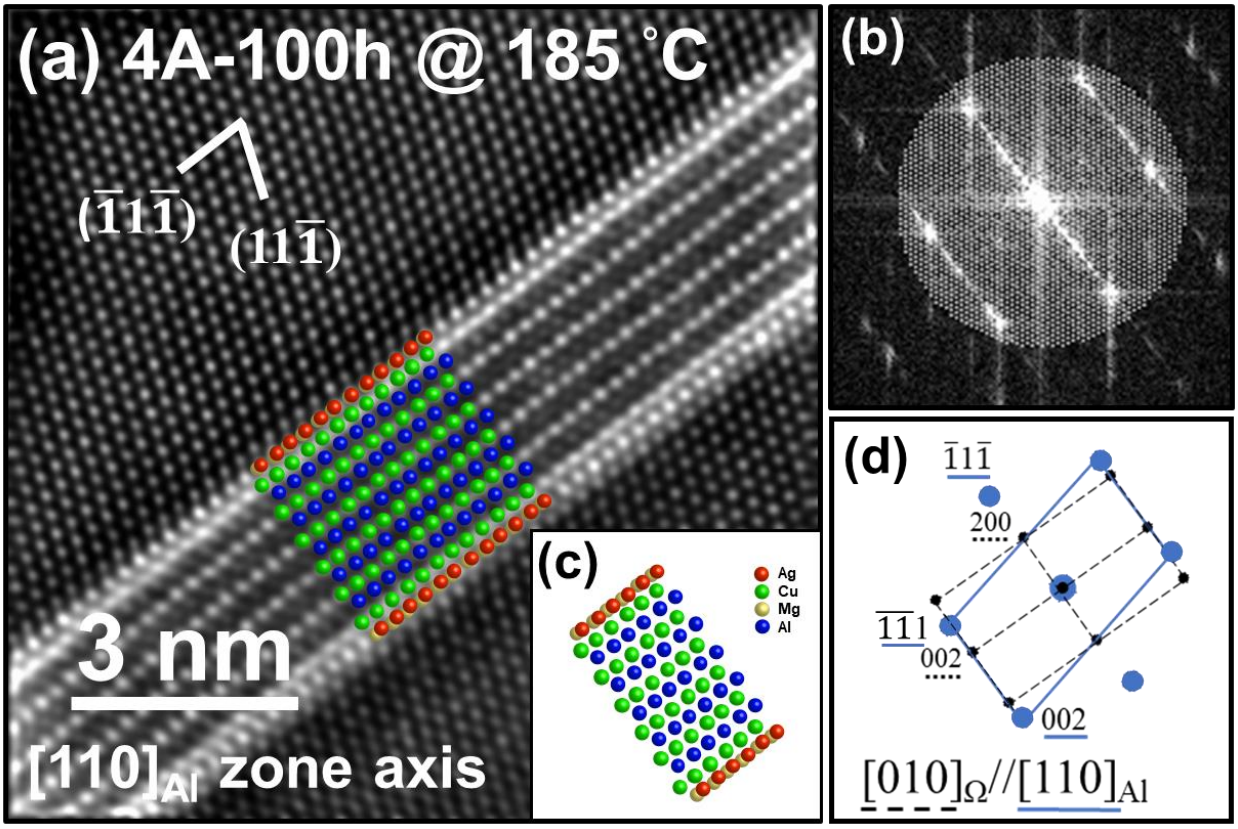


Fig. 8. The Ω phase ageing at 185 °C for 100 h. (a) A filtered HAADF-STEM image with its (b) corresponding FFT diffractograms with the gray circle filter, (c) atomic distribution [28], and (d) simulated diffraction pattern.

4. Discussion

Previous works [15, 21, 22] investigating high Cu/Mg ratio (higher than ~13) 2xxx aluminum alloys indicated that Ag addition triggered the formation of the Ω phase but retarded that of the θ' phase; in addition, the strengthening effect of the Ω phase was presumed to be better than that of the θ' phase. However, the effect of Ag addition on the S phase in the low-ratio Cu/Mg (lower than ~6) alloys has seldom been studied [10, 45, 46]. In the present work, the evolutions of the Ω and S phases and their contributions to the strength from the early ageing stage to the prolonged ageing stage in low Cu/Mg ratio (lower than ~6) AA2024 aluminum alloys have been investigated.

4.1. Relationship between nano-precipitates and mechanical properties

After natural ageing treatment for 4 days, the Ag-free Alloy 0A exhibited a low hardness (93.5 HV). During the initial stage of the artificial ageing, plentiful Cu-Mg clusters presumably formed, resulting in a rapid increment in hardness of ~13% to 105.7 HV in the specimen aged at 185 °C for 1 h, as shown in Fig. 2. As the ageing time reached 5 h, small amounts of S phase could be detected around T phase and on dislocations in the 0A-5h specimen, as shown in Figs. 3a and 6a, increasing the hardness to 124.5 HV and the ultimate tensile strength (UTS) to 401 MPa, as shown in Table 3. After 11 h of ageing, the peak ageing condition (T6) of the Alloy 0A specimen was reached, resulting in the highest hardness (138.5 HV) and UTS (456 MPa). As shown in the TEM images of Figs. 3b and 6b, the rod/lath-like particles of S phase were uniformly distributed in the aluminum matrix, contributing greatly to the strength of alloy 0A. After 18 h of ageing, the TEM images of the 0A-T7 specimen (Figs. 3c and 6c) showed coalesced S phase and large-sized S bundles. At this stage, the UTS declined to 412 MPa, which was ~10% lower than that of the T6 condition. When the ageing time was prolonged to 100 h, the coalescence of the S phase, shown in Figs. 3d and 6d, caused a significant drop in UTS to 326 MPa, which was ~29% lower than that of the T6 condition.

To explore the effects of Ag addition on the evolutions of nano-precipitates and mechanical properties, the Ag-free and Ag-containing samples were compared. In the present work, the Ag-containing Alloy 4A exhibited a hardness (96.4 HV) slightly higher than that of Alloy 0A (93.5

HV) when naturally aged for 4 days. It is appropriate to suggest that, during the initial artificial ageing treatment, Ag diffused into Mg-vacancy clusters to reduce the misfit energy [9], and Ag-Mg clusters are more stable than Cu-Mg cluster because of the larger difference in electronegativity between Ag-Mg than between Cu-Mg [39]. In addition to the formation of Cu-Mg clusters, the formation of plentiful Ag-Mg clusters increased the hardness of the Alloy 4A specimen, rapidly raising it by ~26% to 121.4 HV after ageing for 1 h at 185 °C. This increment was twice that of the Alloy 0A specimen. In the 4A-5h specimen, the Ω phase were ultrathin and uniformly distributed in the aluminum matrix, with a volume percent of 0.29 *vo*l. %, as shown in Figs. 5a and f. The dense Ω phase raised the UTS of 4A-5h specimen to 495 MPa, which was ~23% higher than that of 0A-5h (401 MPa). Alloy 4A reached the peak ageing condition (T6) after 11 h, the same as Alloy 0A, at which ageing time the strength reached 530 MPa, which was ~16 % higher than that of the 0A-T6 specimen (456 MPa). In addition to the similarly-sized S phase in the 0A-T6 and 4A-T6 specimens (Figs. 6b and f), which were presumed to make the same contributions to strength, the higher UTS of 4A-T6 than of 0A-T6 was attributed to the uniform distribution and highest volume percent (4.23 vol. %) of the Ω phase in the aluminum matrix, as shown in Figs. 5b and f. After 18 h of ageing treatment (T7), the strength of the Alloy 4A specimen decreased to 511 MPa. In Figs. 6f and g, the Ω phase adjacent regions were identified as the depleted areas of S phase, implying competition for Cu and Mg with the S phase. The depleted Cu and Mg around the S phase in the 4A-T7 condition

led to its S phase being similar in size to that in the 4A-T6 condition (Figs. 6f and g), and it is presumed that the contributions of the S phase to strength in the 4A-T7 and 4A-T6 specimens were similar. On the other hand, the aspect ratio of the Ω phase in the 4A-T7 specimen became larger, as compared with that of the 4A-T6 specimen. In the 4A-T7 specimen, the average size (diameter) of the Ω phase increased by ~67% and its volume percent decreased to 3.82 vol. %, resulting in a decrease in UTS. However, as compared with the 0A-T7 specimen (~ -10 % UTS decrement relative to the 0A-T6 specimen), the 4A-T7 specimen had a lower decrement in UTS (~ -4 %) than that of the 4A-T6 specimen. It is reasonable to presume that the addition of Ag suppressed the coarsening of the S phase during the longer holding time from 4A-T6 to 4A-T7, and this suppression was also beneficial to the strength. During the long ageing period from 18 h to 100 h, Ω phase which were smaller than a critical size might have dissolved back into the aluminum matrix, and then the dissolved solute atoms diffused into the larger-sized Ω phase; meanwhile, the solute atoms also diffused into the S phase in the vicinity. The competition between the Ω phase and S phase led to a decline of volume percent of the Ω phase and the coarsening of the S phase. After prolonged ageing for 100 h, the volume percent of the Ω phase decreased to 2.74 vol. % (Fig. 5f) and the S phase coalesced (Fig. 6h). The UTS of the 4A-100h specimen decreased by ~ -15% relative to that of the 4A-T6 specimen, falling to 449 MPa. This decrement in Alloy 4A specimen was much smaller than the drop (~ -29%) in UTS between the 0A-100h and 0A-T6 specimens. In addition, the thickness of the thermally stable Ω phase still

remained at around 3 nm after prolonged ageing treatment (100 h) at 185 °C, as shown in Fig. 8a, leading to a nearly constant hardness (~139 HV) after ageing for 80, 90, and 100 h. In contrast, after treatment for the same ageing duration, 0A specimens exhibited a continuous decline in hardness.

4.2. The effect of Ag addition on the S phase

In the Alloy 0A specimens without Ag addition, the sizes of S phase gradually grew and coarsened as the artificial ageing time increased, as shown in Figs. 6a-d. In contrast, in the Alloy 4A specimens, the S phase had no significant difference in size between the T6 and T7 treatments (Figs. 6f and 6g). For further investigation of the evolution of the S phase, the development of the cluster, which is the precursor of the S phase, should also be explored. Previous works have mainly conducted experiments by atom probe tomography (APT) to provide evidence of clusters [15, 26, 45, 57, 71-73]. In the as-quenched condition, Cu-, Mg-, and Ag-vacancy clusters were found independently in Al-1.9Cu-0.3Mg-0.2Ag (at. %) alloy [26]. During the natural ageing stage in Al-3.7Cu-1.6Mg-0.6Mn-0.1Zr-0.04Ti alloy, some Cu-Mg clusters were already formed and thus enhanced the hardness [73]. At the initial stage of artificial ageing at 180 °C for 30 s, plentiful Cu-Mg clusters were observed in Al-1.7Cu-0.3Mg (at %) alloy; however, numerous Ag-Mg clusters were identified in Al-1.9Cu-0.3Mg-0.2Ag (at %) alloy to have formed earlier than Cu-Mg clusters, after treatment at 180 °C for 15 s, due to the stronger affinity between Ag and Mg [26]. In Al-1.1Cu-1.7Mg (at %) alloy [71], as

compared with that in the as-quenched condition, the specimens which were artificially treated at 150 °C for 5 min exhibited much higher hardness (~60 %), being attributed to the formation of large numbers of Cu-Mg clusters. To explore the difference in the evolution of the S phase between Alloys 0A and 4A, a detailed investigation of the nano-scaled clusters as the precursors of S and Ω phases, respectively, needs to be conducted. Here, the preliminary TEM images and their corresponding selected area diffraction (SAD) patterns in the present work are presented in Fig. 9. These high-magnification TEM images show clusters under the observation of $[001]_{Al}$ zone axis of Alloys 0A and 4A specimens aged at 185 °C for 5 h, 11 h (T6), 18 h (T7), and 100 h. Nevertheless, the structure and chemical arrangement of Cu-Mg and Ag-Mg clusters cannot be precisely analyzed without atomic EDS, in addition, no diffraction spots were attributed from these clusters due to their tiny size. In previous works [15, 74] atom probe tomography has shown that Ag-Mg clusters are larger than Cu-Mg clusters. Following the view points from previous works, the present work appropriately identified Cu-Mg and Ag-Mg clusters by comparing the size difference of clusters in the aluminum matrix between Alloys 0A and 4A (the former contains only Cu-Mg clusters, while the latter contains both Cu-Mg and Ag-Mg clusters). The high-magnification TEM image of 0A-5h specimen in Fig. 9a shows ultrafine and uniformly-distributed Cu-Mg clusters with point-like morphology, which were too small to be statistically measured. In addition, the S phase (indicated by red arrows) were rapidly generated on the dislocations rather than in the matrix, as shown in Fig. 9a, for two reasons: the

dislocations stayed in a high energy state that allowed easy nucleation, and the elements could more easily diffuse along the dislocations [74, 75]. In the 0A-T6 and 0A-T7 specimens, as shown in Figs. 9b and c, the Cu-Mg clusters were also uniform in size and distribution, and they tended to grow gradually from 11 h (T6) to 18 h (T7) ageing. It is presumed that the sufficient Cu-Mg clusters in the Al matrix facilitate the growth and coarsening of the S phase, as shown in Figs. 9b and c. Furthermore, the clusters in the matrix of the 0A-100h specimen were significantly larger than those in the 0A-18h specimen, as shown in Fig. 9d. Under the observation of $[001]_{Al}$ zone axis, the HR-TEM image of the 0A-100h specimen (Fig. 10a) revealed the coarse clusters, as indicated by red arrows. From the corresponding Fast Fourier Transform (FFT) diffractogram, the coarse clusters were large enough to contribute to diffraction spots and presumed to be in the form of GPB zone, which was based on the relevant result in previous works [8, 76]. It is suggested that upon prolonged ageing, the initially tiny Cu-Mg clusters gradually transformed into GPB zones, the structure of which still needs to be further investigated. In this stage (in the 0A-100h specimen), the coarse clusters (GPB zones) substitutes for the initially ultrafine Cu-Mg clusters, as shown in Fig. 9d. Unlike in the 0A-5h specimen, large and small clusters co-existed in the 4A-5h specimen, as shown in Fig. 9e. Based on the differences in nanometer-sized clusters between the 0A-5h specimen (Fig. 9a) and 4A-5h specimen (Fig. 9e), it is appropriate to conclude that the large ones were Ag-Mg clusters (indicated by orange circles in Fig. 9e) and the small ones were Cu-Mg clusters, which was

consistent with the results observed by atom probe tomography in previous works [15, 74]. The faster increase in the hardness of Alloy 4A than that of Alloy 0A in the initial stage of 185°C ageing, as shown in Fig. 2, was presumably attributed to the formation of Ag-Mg clusters. After ageing for 11 h, the number of clusters in the 4A-T6 specimen, especially the small-sized Cu-Mg clusters, was reduced, as shown in Fig. 9f. Moreover, small-sized Cu-Mg clusters had almost completely disappeared, and only large Ag-Mg clusters were observed in the aluminum matrix in the 4A-T7 specimen, as shown in Fig. 9g. The HR-TEM image of 4A-T7 in Fig. 10b shows a particle without distinctive diffraction spots in the corresponding FFT diffractograms. The size of this cluster (~3 nm) was close to that of the GPB zone in the 0A-100 h specimen, but this cluster had yet to transform into GPB zone, implying that the cluster was likely an Ag-Mg cluster.

The depletion region between the Ω and S phases as shown in Figs. 6f and g implied the competitive relationship between these two precipitates. The formation of a large volume percent of Ω phase evolved from Ag-Mg clusters consumed much more Cu and Mg atoms than that of the S phase did, causing Cu-Mg clusters to dissolve back into the aluminum matrix and then spread into the Ω phase and Ag-Mg clusters. This triggered the growth of the Ω phase and the formation of new Ω phase, respectively. Unlike the sufficient Cu-Mg clusters in both 0A-T6 and 0A-T7 specimens, the Cu-Mg clusters in the 4A-T6 specimen were sparse and disappeared in the 4A-T7 specimen, leading to suppression of the coarsening of S phase during

this period, as shown in Figs. 6f and g. When the ageing time as prolonged to 100 h, in addition to the Cu-Mg clusters, the Ag-Mg clusters in the aluminum matrix in Fig. 9h were also depleted, resulting in the coalescence of S phase and Ω phase, as shown in Fig. 6h.

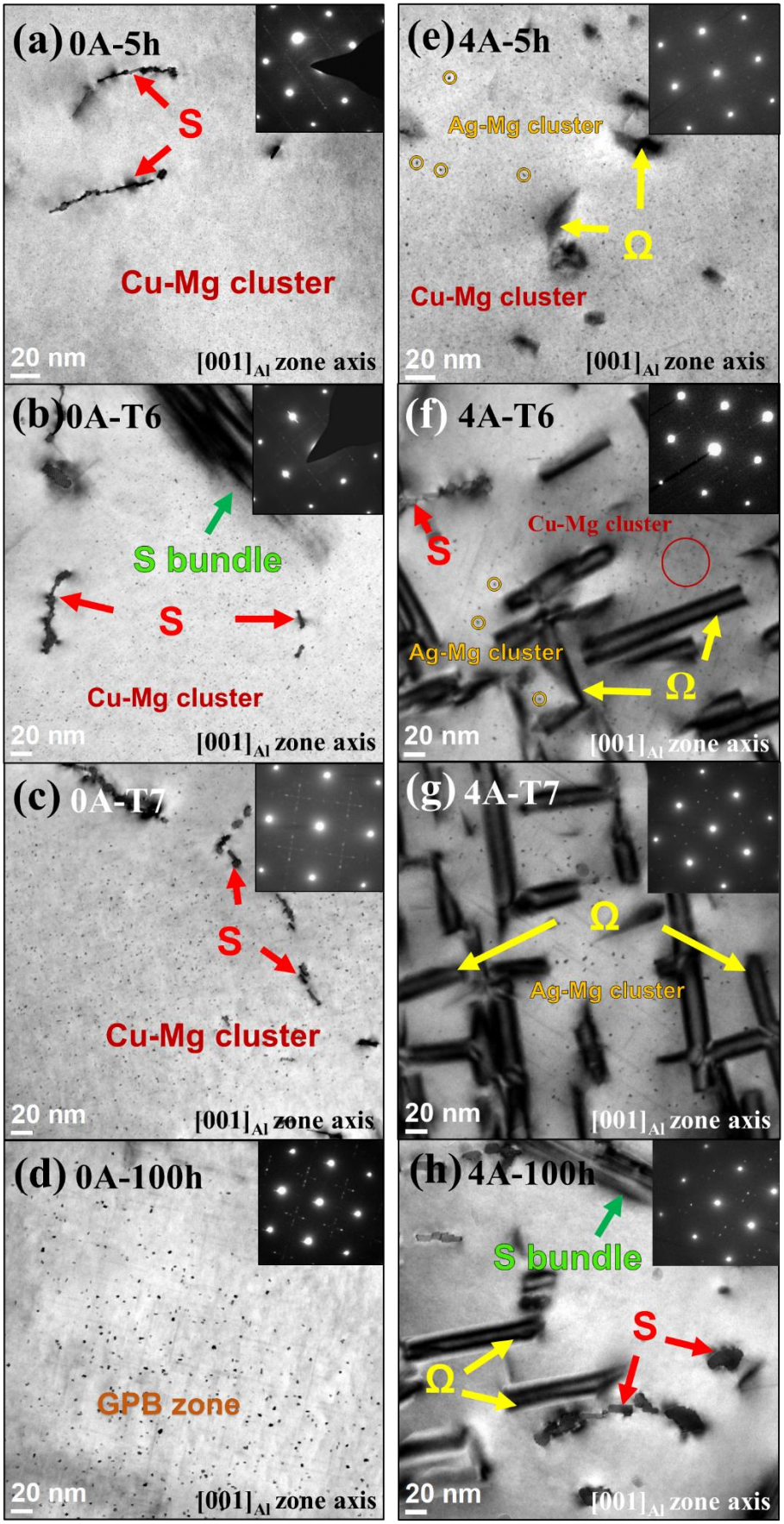


Fig. 9. High magnification TEM images of clusters observed along the $[001]_{Al}$ zone axis in Alloy 0A specimens:(a) 5 h, (b) T6, (c) T7, and (d) 100 h ageing; and Alloy 4A specimens: (e) 5 h, (f) T6, (g) T7, and (h) 100 h ageing.

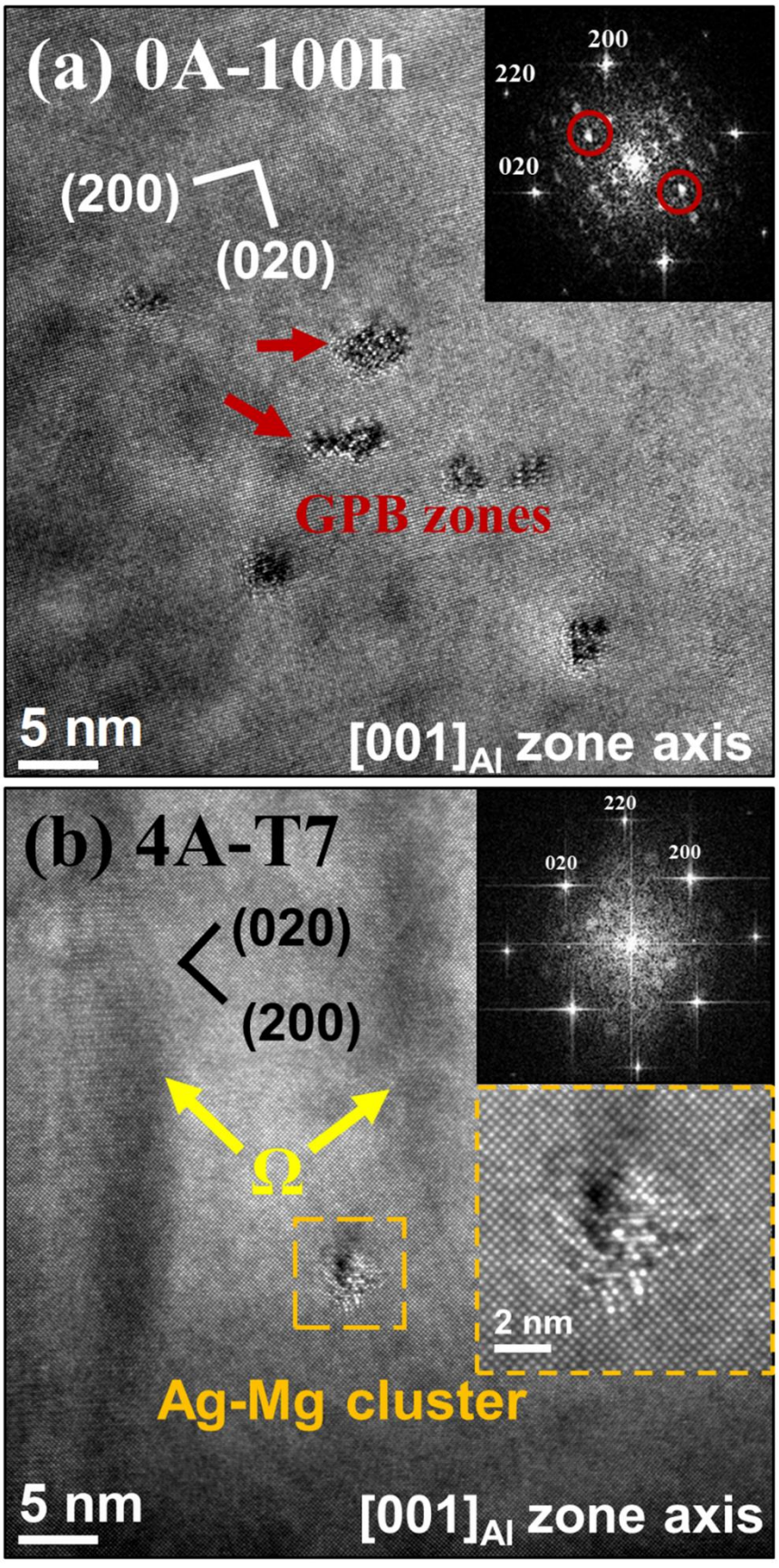


Fig. 10. HR-TEM images with corresponding FFT diffractograms of (a) Cu-Mg clusters observed along the $[001]_{Al}$ zone axis in a 0A-100h specimen and (b) Ag-Mg clusters observed along the $[110]_{Al}$ zone axis in a 4A-T7 specimen.

5. Conclusions

In this work, the microstructural evolutions and mechanical properties of two experimental AA2024 alloys with the same base composition of Al-5.1Cu-1.0Mg (wt%) but different concentrations of Ag, 0 and 0.4 wt. %, respectively denoted as Alloy 0A and Alloy 4A, have been investigated. Both alloys reach the peak ageing condition after T6 ageing treatment at 185 °C for 11 h; the UTS of the 4A-T6 specimen (Alloy 4A treated by T6), 530 MPa, was significantly enhanced to around 16 % higher than that of the 0A-T6 specimen (Alloy 0A treated by T6), 456 MPa. In the over ageing condition of T7, 185 °C for 18 h, the strengths of both alloys decreased; however, as compared with the drop in the UTS of the 0A-T7 specimen (~ -10 %), the decrease in the UTS of the 4A-T7 specimen was only ~ -4 %. The smaller decrement of UTS in the 4A-T7 specimen was presumed to be attributable to the slightly lower volume percent of the Ω phase (3.82 vol. %) and the same size of the S phase particles in comparison with the 4A-T6 specimen. In the 4A-T6 specimens, the minor Ag addition significantly promoted the formation of the Ω phase, consuming more Cu and Mg solute atoms, which led to the depletion of the Cu-Mg in the aluminum matrix, thereby preventing the coarsening of the S phase during the longer holding time from 4A-T6 to 4A-T7. After prolonged ageing at 185 °C for 100 h, the S phase in both alloys coalesced, so the better maintenance of UTS in Alloy 4A (~ -15 %) than in Alloy 0A (~ -29 %) can be confidently attributed to the thermally stable

Ω phase which maintained its high volume percent with thickness of around 3 nm.

Acknowledgments: This work was financially supported by National science and Technology Council, Taiwan under the contract NSTC111-2221-E-002 -155. We would also like to acknowledge the experimental supports from JEOL ARM200F of National Yang Ming Chiao Tung University (NYCU).

Reference

[1] T. Dursun, C. Soutis, Recent developments in advanced aircraft aluminium alloys, Materials & Design (1980-2015) 56 (2014) 862-871.
[2] X. Zhang, Y. Chen, J. Hu, Recent advances in the development of aerospace materials, Progress in Aerospace Sciences 97 (2018) 22-34.
[3] Z. Chen, J. Ren, Z. Yuan, S.P. Ringer, Enhanced strength-plasticity combination in an Al–Cu–Mg alloy——atomic scale microstructure regulation and strengthening mechanisms, Materials Science and Engineering: A 787 (2020) 139447.
[4] S. Ringer, K. Hono, Microstructural evolution and age hardening in aluminium alloys: atom probe field-ion microscopy and transmission electron microscopy studies, Materials characterization 44(1-2) (2000) 101-131.
[5] R. Chester, I. Polmear, TEM investigation of precipitates in AlCuMgAg and AlCuMg alloys, Micron 11(3-4) (1980) 311-312.
[6] I. Polmear, M. Couper, Design and development of an experimental wrought aluminum alloy for use at elevated temperatures, Metallurgical transactions A 19(4) (1988) 1027-1035.
[7] S. Wang, M. Starink, Two types of S phase precipitates in Al–Cu–Mg alloys, Acta Materialia 55(3) (2007) 933-941.
[8] L. Kovarik, S. Court, H. Fraser, M. Mills, GPB zones and composite GPB/GPBII

zones in Al–Cu–Mg alloys, Acta materialia 56(17) (2008) 4804-4815.
[9] B.C. Muddle, I. Polmear, The precipitate Ω phase in Al-Cu-Mg-Ag alloys, Acta Metallurgica 37(3) (1989) 777-789.
[10] C. Macchi, A. Tolley, R. Giovachini, I. Polmear, A. Somoza, Influence of a microalloying addition of Ag on the precipitation kinetics of an Al–Cu–Mg alloy with high Mg: Cu ratio, Acta Materialia 98 (2015) 275-287.
[11] A. Garg, Y. Chang, J. Howe, Precipitation of the Ω phase in an Al-4.0 Cu-0.5 Mg alloy, Scripta Metallurgica et Materialia 24(4) (1990) 677-680.
[12] S. Bai, X. Zhou, Z. Liu, P. Xia, M. Liu, S. Zeng, Effects of Ag variations on the microstructures and mechanical properties of Al–Cu–Mg alloys at elevated temperatures, Materials Science and Engineering: A 611 (2014) 69-76.
[13] M. Song, K.-H. Chen, L.-p. Huang, Effects of Ag addition on mechanical properties and microstructures of Al-8Cu-0.5 Mg alloy, Transactions of Nonferrous Metals Society of China 16(4) (2006) 766-771.
[14] Y. Gu, Z. Liu, D. Yu, B. Liu, M. Lin, S. Zeng, Growth of Ω plates and its effect on mechanical properties in Al-Cu-Mg-Ag alloy with high content of silver, Journal of materials engineering and performance 22(6) (2013) 1708-1715.
[15] S. Bai, P. Ying, Z. Liu, J. Wang, J. Li, Quantitative transmission electron microscopy and atom probe tomography study of Ag-dependent precipitation of Ω phase in Al-Cu-Mg alloys, Materials Science and Engineering: A 687 (2017) 8-16.
[16] J. Vietz, I. Polmear, THE INFLUENCE OF SMALL ADDITIONS OF SILVER ON THE AGEING OF ALUMINIUM ALLOYS.. OBSERVATIONS ON AL-CU-MG ALLOYS, Inst Metals J 94(12) (1966) 410-419.
[17] J.F. Nie, B.C. Muddle, Strengthening of an Al–Cu–Sn alloy by deformation-resistant precipitate plates, Acta Materialia 56(14) (2008) 3490-3501.
[18] J.F. Nie, B.C. Muddle, Microstructural design of high-strength aluminum alloys, Journal of phase equilibria 19(6) (1998) 543-551.
[19] S. Ringer, W. Yeung, B. Muddle, I. Polmear, Precipitate stability in Al・Cu・Mg・Ag alloys aged at high temperatures, Acta metallurgica et materialia 42(5) (1994) 1715-1725.
[20] J. Auld, Structure of metastable precipitate in some Al–Cu–Mg–Ag alloys, Materials science and technology 2(8) (1986) 784-787.
[21] M. Gazizov, R. Kaibyshev, Precipitation structure and strengthening mechanisms in an Al-Cu-Mg-Ag alloy, Materials Science and Engineering: A 702 (2017) 29-40.
[22] X. Zhou, Z. Liu, S. Bai, M. Liu, P. Ying, The influence of various Ag additions on the nucleation and thermal stability of Ω phase in Al–Cu–Mg alloys, Materials Science and Engineering: A 564 (2013) 186-191.
[23] D. Xiao, M. Song, B. Huang, J. Yi, Y. He, Y. Li, Effect of Sc addition on

microstructure and mechanical properties of Al–Cu–Mg–Ag–Zr alloy, Materials Science and Technology 25(6) (2009) 747-752.
[24] L. Reich, M. Murayama, K. Hono, Evolution of Ω phase in an Al–Cu–Mg–Ag alloy—a three-dimensional atom probe study, Acta Materialia 46(17) (1998) 6053-6062.
[25] K. Hono, T. Sakurai, I. Polmear, Pre-precipitate clustering in an Al-Cu-Mg-Ag alloy, Scripta Metallurgica et Materialia;(United States) 30(6) (1994).
[26] S. Ringer, K. Hono, I. Polmear, T. Sakurai, Nucleation of precipitates in aged AlCuMg (Ag) alloys with high Cu: Mg ratios, Acta Materialia 44(5) (1996) 1883-1898.
[27] I. Suh, J.K. Park, Influence of the elastic strain energy on the nucleation of {Omega} phase in Al-Cu-Mg (-Ag) alloys, Scripta metallurgica et materialia 33(2) (1995).
[28] S. Yang, X. Zhao, H. Chen, N. Wilson, J. Nie, Atomic structure and evolution of a precursor phase of Ω precipitate in an Al-Cu-Mg-Ag alloy, Acta Materialia 225 (2022) 117538.
[29] K. Knowles, W. Stobbs, The structure of {111} age-hardening precipitates in Al–Cu–Mg–Ag alloys, Acta Crystallographica Section B: Structural Science 44(3) (1988) 207-227.
[30] J.M. Howe, Analytical transmission electron microscopy analysis of Ag and Mg segregation to {111} θ precipitate plates in an Al-Cu-Mg-Ag alloy, Philosophical magazine letters 70(3) (1994) 111-120.
[31] S.J. Kang, Y.-W. Kim, M. Kim, J.-M. Zuo, Determination of interfacial atomic structure, misfits and energetics of Ω phase in Al–Cu–Mg–Ag alloy, Acta materialia 81 (2014) 501-511.
[32] J. Li, Z. An, F.S. Hage, H. Wang, P. Xie, S. Jin, Q.M. Ramasse, G. Sha, Solute clustering and precipitation in an Al–Cu–Mg–Ag–Si model alloy, Materials Science and Engineering: A 760 (2019) 366-376.
[33] S.J. Kang, Y.-W. Kim, M. Kim, J.-M. Zuo, Interfacial microscopic mechanism of free energy minimization in Omega precipitate formation, arXiv preprint arXiv:1401.6731 (2014).
[34] S. Yang, N. Wilson, J. Nie, Revisit of the structure of Ω precipitate in Al-Cu-Mg-Ag alloys, Scripta Materialia 205 (2021) 114204.
[35] Z. Huda, N.I. Taib, T. Zaharinie, Characterization of 2024-T3: An aerospace aluminum alloy, Materials Chemistry and Physics 113(2-3) (2009) 515-517.
[36] Y. Chen, J. Feng, H. Liu, Precipitate evolution in friction stir welding of 2219-T6 aluminum alloys, Materials characterization 60(6) (2009) 476-481.
[37] Y. Chang, J. Howe, Composition and stability of Ω phase in an Al-Cu-Mg-Ag alloy, Metallurgical Transactions A 24(7) (1993) 1461-1470.
[38] J. Taylor, B. Parker, I. Polmear, Precipitation in AI-Cu-Mg-Ag casting alloy, Metal Science 12(10) (1978) 478-482.

[39] Y.-T. Chen, G.-Y. Nieh, J.-H. Wang, T.-F. Wu, S.-L. Lee, Effects of Cu/Mg ratio and heat treatment on microstructures and mechanical properties of Al–4.6 Cu–Mg–0.5 Ag alloys, Materials Chemistry and Physics 162 (2015) 764-770.
[40] Q. Cui, G. Itoh, M. Kanno, Effect of silver addition on the precipitation of the Ω-phase in an Al-Cu-Mg alloy, Nippon Kinzoku Gakkaishi (1952) 59(5) (1995) 492-501.
[41] C.R. Hutchinson, X. Fan, S.J. Pennycook, G.J. Shiflet, On the origin of the high coarsening resistance of Ω plates in Al–Cu–Mg–Ag alloys, Acta materialia 49(14) (2001) 2827-2841.
[42] B. Li, F. Wawner, Dislocation interaction with semicoherent precipitates (Ω phase) in deformed Al–Cu–Mg–Ag alloy, Acta materialia 46(15) (1998) 5483-5490.
[43] S. Bai, H. Di, Z. Liu, Dislocation interaction with Ω phase in crept Al–Cu–Mg–Ag alloys, Materials Science and Engineering: A 651 (2016) 399-405.
[44] J. da Costa Teixeira, D.G. Cram, L. Bourgeois, T.J. Bastow, A.J. Hill, C. Hutchinson, On the strengthening response of aluminum alloys containing shear-resistant plate-shaped precipitates, Acta materialia 56(20) (2008) 6109-6122.
[45] S. Bai, Z. Liu, X. Zhou, P. Xia, S. Zeng, Mg-controlled formation of Mg–Ag co-clusters in initial aged Al–Cu–Mg–Ag alloys, Journal of Alloys and Compounds 602 (2014) 193-198.
[46] A. Al-Obaisi, E. El-Danaf, A. Ragab, M. Soliman, Precipitation hardening and statistical modeling of the aging parameters and alloy compositions in Al-Cu-Mg-Ag alloys, Journal of Materials Engineering and Performance 25(6) (2016) 2432-2444.
[47] J. Liu, S. Yang, S. Wang, J. Chen, C. Wu, The influence of Cu/Mg atomic ratios on precipitation scenarios and mechanical properties of Al–Cu–Mg alloys, Journal of alloys and compounds 613 (2014) 139-142.
[48] L. Liu, J. Chen, S. Wang, C. Liu, S. Yang, C. Wu, The effect of Si on precipitation in Al–Cu–Mg alloy with a high Cu/Mg ratio, Materials Science and Engineering: A 606 (2014) 187-195.
[49] C. Pan, Y. Yang, S. Wang, Y. Liu, S. Hu, Z. Wang, P. Shen, Atomistic building blocks of one-dimensional Guinier–Preston–Bagaryatsky zones in Al-Cu-Mg alloys, Materials & Design 187 (2020) 108393.
[50] M. Mohedano, M. Serdechnova, M. Starykevich, S. Karpushenkov, A. Bouali, M. Ferreira, M. Zheludkevich, Active protective PEO coatings on AA2024: Role of voltage on in-situ LDH growth, Materials & Design 120 (2017) 36-46.
[51] Y.A. Bagaryatsky, Structural changes on aging Al-Cu-Mg alloys, Dokl Akad SSSR, 1952, pp. 397-559.
[52] R. Wilson, P. Partridge, The nucleation and growth of S'precipitates in an aluminium-2.5% copper-1.2% magnesium alloy, Acta Metallurgica 13(12) (1965) 1321-1327.

[53] S.P. Ringer, T. Sakurai, I. Polmear, Origins of hardening in aged Al・Gu・Mg・(Ag) alloys, Acta materialia 45(9) (1997) 3731-3744.
[54] J.K. Sunde, D.N. Johnstone, S. Wenner, A.T. van Helvoort, P.A. Midgley, R. Holmestad, Crystallographic relationships of T-/S-phase aggregates in an Al–Cu–Mg–Ag alloy, Acta Materialia 166 (2019) 587-596.
[55] Y. Chen, S. Pan, B. Zhu, X. Liu, W. Liu, S. Tang, The evolution of orientation relationships during the transformation of a twin-free T-particle to tenfold T-twins in an Al alloy during homogenisation, Materials Characterization 141 (2018) 59-73.
[56] S. Ringer, B. Sofyan, K. Prasad, G. Quan, Precipitation reactions in Al–4.0 Cu–0.3 Mg (wt.%) alloy, Acta Materialia 56(9) (2008) 2147-2160.
[57] G. Sha, R. Marceau, X. Gao, B. Muddle, S. Ringer, Nanostructure of aluminium alloy 2024: Segregation, clustering and precipitation processes, Acta Materialia 59(4) (2011) 1659-1670.
[58] S. Wang, M. Starink, N. Gao, Precipitation hardening in Al–Cu–Mg alloys revisited, Scripta Materialia 54(2) (2006) 287-291.
[59] S. Wang, M. Starink, The assessment of GPB2/S〞〞 structures in Al–Cu–Mg alloys, Materials Science and Engineering: A 386(1-2) (2004) 156-163.
[60] A. Charai, T. Walther, C. Alfonso, A.-M. Zahra, C. Zahra, Coexistence of clusters, GPB zones, S〃-, S〞-and S-phases in an Al–0.9% Cu–1.4% Mg alloy, Acta materialia 48(10) (2000) 2751-2764.
[61] Z. Liu, J. Chen, S. Wang, D. Yuan, M. Yin, C. Wu, The structure and the properties of S-phase in AlCuMg alloys, Acta materialia 59(19) (2011) 7396-7405.
[62] J.K. Sunde, D.N. Johnstone, S. Wenner, A.T.J. van Helvoort, P.A. Midgley, R. Holmestad, Crystallographic relationships of T-/S-phase aggregates in an Al-Cu-Mg-Ag alloy, Acta Materialia 166 (2019) 587-596.
[63] M.J. Styles, C. Hutchinson, Y. Chen, A. Deschamps, T.J. Bastow, The coexistence of two S (Al2CuMg) phases in Al–Cu–Mg alloys, Acta materialia 60(20) (2012) 6940-6951.
[64] M.J. Styles, R.K.W. Marceau, T.J. Bastow, H.E. Brand, M.A. Gibson, C.R. Hutchinson, The competition between metastable and equilibrium S (Al2CuMg) phase during the decomposition of AlCuMg alloys, Acta Materialia 98 (2015) 64-80.
[65] T. Malis, S. Cheng, R. Egerton, EELS log-ratio technique for specimen-thickness measurement in the TEM, Journal of electron microscopy technique 8(2) (1988) 193-200.
[66] H.-W. Yen, P.-Y. Chen, C.-Y. Huang, J.-R. Yang, Interphase precipitation of nanometer-sized carbides in a titanium–molybdenum-bearing low-carbon steel, Acta Materialia 59(16) (2011) 6264-6274.
[67] N. Radutoiu, L. Lacroix, J. Alexis, M. Abrudeanu, J.-A. Petit, Study of the localized

corrosion of over-aged aeronautical 2024 aluminum alloy. Kelvin probe Force Microscopy (KFM) application, ACMA 2012, 2012.
[68] C. Li, Q. Pan, Y. Shi, Y. Wang, B. Li, Influence of aging temperature on corrosion behavior of Al–Zn–Mg–Sc–Zr alloy, Materials & Design 55 (2014) 551-559.
[69] X. Guo, Y. Deng, X. Zhang, Quantitative study of the effect of stress on the precipitation in an Al-Cu-Mg-Ag alloy single crystal, Materials Science and Engineering: A 730 (2018) 187-196.
[70] M. Gazizov, R. Kaibyshev, Effect of pre-straining on the aging behavior and mechanical properties of an Al–Cu–Mg–Ag alloy, Materials Science and Engineering: A 625 (2015) 119-130.
[71] S.P. Ringer, K. Hono, T. Sakurai, I.J. Polmear, Cluster hardening in an aged Al-Cu-Mg alloy, Scripta materialia 36(5) (1997) 517-521.
[72] R.K. Marceau, G. Sha, R. Lumley, S.P. Ringer, Evolution of solute clustering in Al–Cu–Mg alloys during secondary ageing, Acta materialia 58(5) (2010) 1795-1805.
[73] P. Ying, Z. Liu, S. Bai, M. Liu, L. Lin, P. Xia, L. Xia, Effects of pre-strain on Cu-Mg co-clustering and mechanical behavior in a naturally aged Al-Cu-Mg alloy, Materials Science and Engineering: A 704 (2017) 18-24.
[74] S. Bai, X. Yi, Z. Liu, J. Wang, J. Zhao, P. Ying, The influence of preaging on the strength and precipitation behavior of a deformed Al-Cu-Mg-Ag alloy, Journal of Alloys and Compounds 764 (2018) 62-72.
[75] P. Ratchev, B. Verlinden, P. De Smet, P. Van Houtte, Precipitation hardening of anAl–4.2 wt% Mg–0.6 wt% Cu alloy, Acta materialia 46(10) (1998) 3523-3533.
[76] L. Kovarik, M. Mills, STEM HAADF Observations of GPB zones in Al-Cu-Mg alloys, Microscopy and Microanalysis 13(S02) (2007) 1064-1065.